

Finite-temperature dynamical structure factor of the Heisenberg-Ising chain

A. J. A. James,^{1,2} W. D. Goetze,² and F. H. L. Essler²

¹*Department of Physics, University of Virginia, Charlottesville, Virginia 22904-4717, USA*

²*Rudolf Peierls Centre for Theoretical Physics, University of Oxford, Oxford OX1 3NP, United Kingdom*

(Received 4 March 2009; published 9 June 2009)

We consider the spin-1/2 Heisenberg XXZ chain in the regime of large Ising-type anisotropy Δ . By a combination of duality and Jordan-Wigner transformations we derive a mapping to weakly interacting spinless fermions, which represent domain walls between the two degenerate ground states. We develop a perturbative expansion in $1/\Delta$ for the transverse dynamical spin structure factor at finite temperatures and in an applied transverse magnetic field. We present a unified description for both the low-energy temperature-activated response and the temperature evolution of the $T=0$ two-spinon continuum. We find that the two-spinon continuum *narrows* in energy with increasing temperature. At the same time spectral weight is transferred from the two-spinon continuum to the low-energy intraband scattering continuum, which is strongly peaked around the position of the (single) spinon dispersion (“Villain mode”).

DOI: 10.1103/PhysRevB.79.214408

PACS number(s): 75.10.Jm, 75.10.Pq, 75.40.Gb

I. INTRODUCTION

The spin-1/2 Heisenberg XXZ chain is a paradigm in low-dimensional quantum magnetism. Its Hamiltonian is

$$H = J \sum_n \Delta S_n^z S_{n+1}^z + S_n^x S_{n+1}^x + S_n^y S_{n+1}^y + \sum_n \mathbf{h} \cdot \mathbf{S}_n, \quad (1)$$

where \mathbf{h} is an external magnetic field and Δ controls the exchange anisotropy. The one-dimensional case is particularly significant because for a field \mathbf{h} parallel to the \hat{z} direction, the Hamiltonian is integrable and the spectrum of the spin chain may be extracted exactly.^{1–4} Furthermore the Hamiltonian (1) is thought to provide a realistic description of several quasi-one-dimensional (1D) experimental compounds. Examples include Cs_2CoCl_4 for which $\Delta=0.25$,^{5–7} CsCoBr_3 ,^{8,9} CsCoCl_3 ,¹⁰ and TlCoCl_3 (Ref. 11) all of which have $\Delta \sim 7$.

For $\Delta > 1$, $h=0$, and $T=0$ the XXZ spin chain is in a Néel phase. The fundamental excitations take the form of gapped fractionalized spin-1/2 quantum solitons known as spinons.¹² Strictly in the Ising limit, $\Delta=\infty$, the spinons can be identified simply as domain walls with gap $\Delta/2$. Experiments have established the existence of several manifestations of the XXZ model in the Ising regime.^{8–11} In some cases these experiments have also probed the effects of temperature^{9,13} and transverse field¹³ on dynamical spin-spin correlations.

The measure of dynamical correlations known as the dynamical structure factor (DSF) is an important quantity in the study of quantum magnets.¹⁴ This is for two reasons: first, the dynamical structure factor is directly measurable by inelastic neutron-scattering experiments and second, the nature of the dynamical response is highly specific to the system in question, so that it serves as a characterization tool. A particular feature that one would like to understand in the case of the XXZ chain is the finite-temperature low-energy spin response known as the “Villain mode.”¹⁵ This response due to scattering between domain-wall pair states has been observed in Refs. 9 and 13. As this response occurs only at finite temperatures it necessitates a theory that accounts for thermal fluctuations. A recent analysis of the continuum limit

of two gapped integrable quantum spin chains¹⁶ has shown that at raised temperatures the effect of thermal fluctuations cannot be described in terms of a simple thermal decoherence or relaxation-time picture. Instead markedly asymmetric thermal broadening of single-particle modes is observed. This paradigm has been found to be in agreement with theoretical^{17,18} and experimental¹⁹ studies of the spin-1/2 Heisenberg chain with strongly alternating exchange, a model which is gapped but not integrable. In contrast the gapped excitations in the spin-1/2 XXZ chain occur only in pairs; it is then interesting to try and understand the thermal evolution of the resulting two particle response in addition to that of the Villain mode.

Despite the advantages afforded by integrability, the task of calculating correlation functions (and hence dynamics) for spin chains is still far from simple. For example, the case $\Delta=0$, $\mathbf{h}=(0,0,h)$ corresponds to the XY chain with a finite field in the z direction, for which the excitations are described exactly by noninteracting spinless fermions.²⁰ This allows one to calculate the two-point function of S^z by elementary means even for $T>0$.²¹ On the other hand the determination of transverse correlations is a nontrivial problem.^{22,23}

For the XXZ chain first-order perturbative treatments around the $\Delta=\infty$ limit^{8,15,24} and $1/S$ expansions²⁵ have given some insight. In recent years significant progress has been made for the $\Delta > 1$ regime, both via Bethe’s Ansatz²⁶ and a different exact technique which works directly with the thermodynamic limit.²⁷ This has led to an exact expression for the transverse dynamical correlations at $T=0$.^{26,28} Results at finite temperature are generally still limited to asymptotically exact thermodynamic quantities.^{29–32} However there have been promising advances that rely on generalizing multiple integral representations for time-dependent correlation functions to finite temperatures.^{33–36} Currently these methods have not yielded expressions for the most experimentally relevant quantity—the dynamical structure factor.

In this paper we present a perturbative calculation for the transverse spin response in the $\Delta \gg 1$ limit, valid at finite temperatures and capable of incorporating a transverse field. We note that the temperature dependence of the dynamical

structure factor in the critical $-1 < \Delta \leq 1$ regime has been determined by exact diagonalization of short chains and very recently by quantum Monte Carlo and density matrix renormalization group (DMRG) computations.³⁷ The usual perturbative approach to the XXZ chain uses the Jordan-Wigner transformation³⁸ to produce an expansion in powers of Δ . This is suitable for investigating the XY phase, $|\Delta| \ll 1$, but inadequate here. Instead we first perform a Kramers-Wannier³⁹ duality transformation to a new Hamiltonian in terms of dual operators. A Jordan-Wigner transformation from these dual operators to spinless fermions then leads to a controlled expansion in $1/\Delta$. An equivalent mapping has been used previously, coupled with mean-field theory, to find the approximate excitation spectrum in the Ising phase.⁴⁰ We take an alternative approach resumming certain terms in the expansion to all orders in order to take account of both quantum and thermal fluctuations.

The structure of the paper is as follows. First in Sec. II we discuss symmetries of the Hamiltonian and the dynamical structure factor. Second, in Sec. III we transform the Hamiltonian into a form suitable for the expansion. In Sec. IV we describe the perturbative expansion of the transverse spin-spin correlator. In Sec. V we explain how to resum certain terms in this expansion in order to obtain finite results. In Sec. VI we discuss the behavior of the dynamical structure factor for a range of parameters. Section VIII contains some brief concluding remarks.

II. SYMMETRIES OF THE HAMILTONIAN AND THE STRUCTURE FACTOR

We now describe the symmetries of the Hamiltonian and their consequences for spin-spin correlation functions. For $h=0$ the Hamiltonian, Eq. (1), is invariant under arbitrary rotations $\mathcal{R}^z(\phi)$ around the z axis as well as under rotations by π around the x axis, $\mathcal{R}^x(\pi)$, which entail the mapping

$$S_j^x \rightarrow S_j^x, \\ S_j^{y,z} \rightarrow -S_j^{y,z}.$$

The two types of symmetry operations do not commute, but we can diagonalize the Hamiltonian simultaneously with either S^z or with the generator $\mathcal{R}^x(\pi)$ of the \mathbb{Z}_2 symmetry. This in turn implies that all off-diagonal spin correlators vanish for $T > 0$ by the following arguments. When considering the thermal expectation values $\langle S_n^a S_m^z \rangle$, with $a=x,y$, we choose a basis of energy eigenstates in which the total S^z is diagonal. Then carrying out a rotation by π around the z axis sends $S_n^a \rightarrow -S_n^a$, $a=x,y$, and as a result

$$\langle S_n^a S_m^z \rangle = -\langle S_n^a S_m^z \rangle = 0, \quad a=x,y. \quad (2)$$

On the other hand, when considering $\langle S_n^x S_m^y \rangle$ we use a basis of simultaneous eigenstates of H and $\mathcal{R}^x(\pi)$ to carry out the thermal trace. Under the \mathbb{Z}_2 symmetry the thermal expectation value is negated, leading to

$$\langle S_n^x S_m^y \rangle = -\langle S_n^x S_m^y \rangle = 0. \quad (3)$$

This shows that in the absence of the transverse magnetic field all off-diagonal elements of the dynamical structure fac-

tor vanish. In the presence of a finite transverse field we only have the \mathbb{Z}_2 to work with. Concomitantly for $h > 0$ one finds $\langle S_n^x S_m^y \rangle = \langle S_n^x S_m^z \rangle = 0$ but $\langle S_n^y S_m^z \rangle$ is no longer required to vanish by symmetry and as a result acquires a finite value.

III. TRANSFORMATIONS OF THE HAMILTONIAN

In order to proceed we aim to re-express the Hamiltonian in terms of spinless fermions by means of a Jordan-Wigner transformation in such a way that we analyze the resulting interacting fermion Hamiltonian by standard perturbative methods. In order to achieve this, the $\Delta J \sum_n S_n^z S_{n+1}^z$ part of the Hamiltonian (1) must be mapped to an expression quadratic in fermions. One approach for doing this is outlined in Appendix A, another one is discussed in detail next. In the following we consider a *transverse* magnetic field applied along the \hat{x} direction. We note that the effects of a transverse field in the critical region of the XXZ chain $-1 < \Delta \leq 1$ have been studied in some detail in Ref. 41.

A. Duality transformation

We work on the infinite chain so that we can ignore boundary effects. The Hamiltonian, Eq. (1), in terms of Pauli-spin matrices is given by

$$H = H_\Delta + H_h,$$

$$H_\Delta = \frac{J}{4} \Delta \sum_n \sigma_n^z \sigma_{n+1}^z + \frac{J}{4} \sum_n (\sigma_n^x \sigma_{n+1}^x + \sigma_n^y \sigma_{n+1}^y),$$

$$H_h = \frac{h}{2} \sum_n \sigma_n^x. \quad (4)$$

The Kramers-Wannier duality transformation is defined by

$$\mu_{n+1/2}^x = \sigma_n^z \sigma_{n+1}^z, \quad \mu_{n+1/2}^z = \prod_{j < n+1} \sigma_j^x, \\ \mu_{n+1/2}^y = -i \mu_{n+1/2}^z \mu_{n+1/2}^x. \quad (5)$$

This transformation defines operators on a dual lattice and maps an Ising chain from its ordered to its disordered phase.⁴² Applying the transformation to the XXZ Hamiltonian we find

$$H_\Delta = \frac{J}{4} \sum_n (\Delta \mu_{n+1/2}^x + \mu_{n-1/2}^z \mu_{n+3/2}^z - \mu_{n+1/2}^x \mu_{n-1/2}^z \mu_{n+3/2}^z), \\ H_h = \frac{h}{2} \sum_n \mu_{n-1/2}^z \mu_{n+1/2}^z. \quad (6)$$

We note that applying the duality transformation to a finite open chain leads to a dual Hamiltonian containing additional boundary terms that in particular ensure a doubly-degenerate ground state in the thermodynamic limit. This is most easily seen for $\Delta \gg h \gg 1$, i.e., the Ising model in a transverse field. In this limit the mapping gives

$$\begin{aligned} & \Delta \sum_{n=1}^{N-1} \sigma_n^z \sigma_{n+1}^z + h \sum_{n=1}^N \sigma_n^x \\ & \rightarrow h \sum_{n=1}^{N-1} \mu_{n+1/2}^z \mu_{n+3/2}^z + \Delta \sum_{n=1}^{N-1} \mu_{n+1/2}^x + h \mu_{3/2}^z. \end{aligned} \quad (7)$$

Now as $h/\Delta \rightarrow 0$ the two ground states of the original Hamiltonian become the familiar Néel states, $\langle \sigma_n^z \rangle = -\langle \sigma_{n+1}^z \rangle$. In contrast, for the dual Hamiltonian the ground state is given by $\langle \mu_{n+1/2}^x \rangle = -1$ with $n < N$. The twofold degeneracy is then maintained by the N th dual spin, $\mu_{N+1/2}$, which is free to point in either direction. In the following we will be interested only in bulk correlations of operators that are local under the duality transformation. Hence the boundary terms do not play a role and will be dropped.

B. Fermionic representation

In order to proceed further it is necessary to map the spins to fermions. We perform a rotation of spin axes about the (1, 1) direction

$$\mu_{n+1/2}^x \rightarrow \tau_n^z, \quad \mu_{n+1/2}^z \rightarrow \tau_n^y, \quad (8)$$

with raising and lowering operators

$$\tau_n^+ = \frac{\tau_n^x + i\tau_n^y}{2}, \quad \tau_n^- = \frac{\tau_n^x - i\tau_n^y}{2}, \quad (9)$$

and then use the Jordan-Wigner transformation

$$\begin{aligned} \tau_n^z &= 2c_n^\dagger c_n - 1, \\ \tau_n^+ &= c_n^\dagger \exp\left(-i\pi \sum_{j<n} c_j^\dagger c_j\right). \end{aligned} \quad (10)$$

1. Spin operators

We first consider the transformation of the lattice spin operators under the mappings. Crucially, the transverse spin operator is local under the transformations

$$\sigma_n^x = c_{n-1}^\dagger c_n - c_{n-1}^\dagger c_n^\dagger + \text{H.c.} \quad (11)$$

On the other hand, both σ^z and σ^y acquire Jordan-Wigner strings. As a result, our formalism will allow us to determine the xx component of the dynamical structure factor only. It follows from the symmetry considerations above that in absence of a transverse magnetic field this suffices to determine all transverse correlations.

2. Hamiltonian

After the Jordan-Wigner transformation the Hamiltonian takes the form

$$\begin{aligned} H_\Delta &= \frac{J}{2} \Delta \sum_n c_n^\dagger c_n + \frac{J}{2} \sum_n [c_{n-1}^\dagger c_{n+1} - c_{n-1}^\dagger c_{n+1}^\dagger \\ & - c_{n-1}^\dagger c_n^\dagger c_n c_{n+1} + c_{n-1}^\dagger c_n^\dagger c_n c_{n+1}^\dagger + \text{H.c.}] + \text{const} \end{aligned} \quad (12)$$

and

$$H_h = \frac{h}{2} \sum_n (c_{n-1}^\dagger c_n - c_{n-1}^\dagger c_n^\dagger + \text{H.c.}). \quad (13)$$

We now write the Hamiltonian as a sum of two pieces, $H = H_2 + H_4$, containing quadratic and quartic terms in the fermionic operators, respectively. The quartic (interaction) terms are $\mathcal{O}(\Delta^0)$ while the quadratic pieces mix orders $\mathcal{O}(\Delta)$ and $\mathcal{O}(\Delta^0)$. The external field only appears in the quadratic part of the Hamiltonian. After taking the Fourier transform of the quadratic part, H_2 , of the Hamiltonian we find

$$H_2 = \frac{J}{8} \sum_k (c_k^\dagger \ c_{-k}) \begin{pmatrix} A_k & iB_k \\ -iB_k & -A_k \end{pmatrix} \begin{pmatrix} c_k \\ c_{-k}^\dagger \end{pmatrix}, \quad (14)$$

with $A_k = 2\Delta + 4 \cos(2k) + \frac{4h}{J} \cos(k)$ and $B_k = 4 \sin(2k) + \frac{4h}{J} \sin(k)$. This can be diagonalized by a Bogoliubov transformation of the form

$$\begin{pmatrix} c_k \\ c_{-k}^\dagger \end{pmatrix} = \begin{pmatrix} i \cos(\theta_k) & -\sin(\theta_k) \\ \sin(\theta_k) & -i \cos(\theta_k) \end{pmatrix} \begin{pmatrix} \alpha_k \\ \alpha_{-k}^\dagger \end{pmatrix}, \quad (15)$$

so that

$$H_2 = \frac{1}{2} \sum_k (\alpha_k^\dagger \ \alpha_{-k}) \begin{pmatrix} \epsilon_k & 0 \\ 0 & -\epsilon_k \end{pmatrix} \begin{pmatrix} \alpha_k \\ \alpha_{-k}^\dagger \end{pmatrix}, \quad (16)$$

with $\tan(2\theta_k) = B_k/A_k$ and $\epsilon_k = \frac{J}{4} \sqrt{A_k^2 + B_k^2}$.

Now we consider the quartic part of the Hamiltonian

$$H_4 = -\frac{J}{2} \sum_n (c_{n-1}^\dagger c_n^\dagger c_n c_{n+1} + c_{n-1}^\dagger c_n^\dagger c_{n+1}^\dagger c_n + \text{H.c.}). \quad (17)$$

Taking the Fourier transform and manipulating indices leads to

$$\begin{aligned} H_4 &= -\frac{J}{4N} \sum_{k_1, k_2, k_3, k_4} \delta_{k_1+k_2+k_3+k_4} \left[f_{(k_1, k_2)(k_3, k_4)} c_{k_1}^\dagger c_{k_2}^\dagger c_{-k_3} c_{-k_4} \right. \\ & \left. + \frac{2}{3} (i g_{(k_1, k_2, k_3)} c_{k_1}^\dagger c_{k_2}^\dagger c_{k_3}^\dagger c_{-k_4} + \text{H.c.}) \right], \end{aligned} \quad (18)$$

where we have defined the new functions

$$\begin{aligned} f_{(k_1, k_2)(k_3, k_4)} &= \cos(k_1 - k_4) - \cos(k_2 - k_4) \\ & - \cos(k_1 - k_3) + \cos(k_2 - k_3), \end{aligned} \quad (19)$$

$$g_{(k_1, k_2, k_3)} = \sin(k_1 - k_2) + \sin(k_2 - k_3) + \sin(k_3 - k_1). \quad (20)$$

The function f is antisymmetric under exchange of the two momenta within a pair of brackets. The function g is symmetric for cyclic permutations of its momentum arguments and antisymmetric otherwise. For example, $f_{(k_1, k_2)(k_3, k_4)} = -f_{(k_2, k_1)(k_3, k_4)} = f_{(k_3, k_4)(k_1, k_2)}$ and $g_{(k_1, k_2, k_3)} = g_{(k_2, k_3, k_1)} = -g_{(k_2, k_1, k_3)}$. Performing the Bogoliubov transformation on H_4 is standard but lengthy. By manipulating indices under the sums we arrive at a relatively compact form for the part quartic in Bogoliubov operators

$$\begin{aligned}
 H_4 = & \frac{1}{N} \sum_{1,2,3,4} \delta_{k_1+k_2+k_3+k_4,0} \{ V_0(k_1, k_2, k_3, k_4) [\alpha_{k_1}^\dagger \alpha_{k_2}^\dagger \alpha_{k_3}^\dagger \alpha_{k_4}^\dagger \\
 & + \text{H.c.}] + [V_1(k_1, k_2, k_3, k_4) \alpha_{k_1}^\dagger \alpha_{-k_2} \alpha_{-k_3} \alpha_{-k_4} + \text{H.c.}] \\
 & + V_2(k_1, k_2, k_3, k_4) \alpha_{k_1}^\dagger \alpha_{k_2}^\dagger \alpha_{-k_3} \alpha_{-k_4} \}. \quad (21)
 \end{aligned}$$

The interaction vertices are given by

$$\begin{aligned}
 V_0(k_1, k_2, k_3, k_4) = & \frac{J}{96} \sum_{P \in \mathcal{S}_4} \text{sgn}(P) \cos(k_{P(1)} - k_{P(2)} - \theta_{k_{P(1)}} \\
 & + \theta_{k_{P(2)}} + \theta_{k_{P(3)}} - \theta_{k_{P(4)}}), \quad (22)
 \end{aligned}$$

with permutation P acting on the set $\{1,2,3,4\}$,

$$\begin{aligned}
 V_1(k_1, k_2, k_3, k_4) = & i \frac{J}{12} \sum_{P \in \mathcal{S}_3} \text{sgn}(P) [\sin(k_1 - k_{P(2)} - \theta_{k_1} + \theta_{k_{P(2)}} \\
 & + \theta_{k_{P(3)}} - \theta_{k_{P(4)}}) - \sin(k_{P(2)} - k_{P(3)} + \theta_{k_1} \\
 & - \theta_{k_{P(2)}} + \theta_{k_{P(3)}} - \theta_{k_{P(4)}})], \quad (23)
 \end{aligned}$$

with permutation P acting on the set $\{2,3,4\}$ and finally

$$\begin{aligned}
 V_2(k_1, k_2, k_3, k_4) = & \frac{J}{8} \left(\sum_{P \in \mathcal{S}_3} \text{sgn}(P) \cos(k_3 - k_4 - \theta_{k_3} + \theta_{k_4} \right. \\
 & - \theta_{k_{P(1)}} + \theta_{k_{P(2)}}) + \sum_{P' \in \mathcal{S}_3} \text{sgn}(P') \cos(k_1 - k_2 \\
 & - \theta_{k_1} + \theta_{k_2} - \theta_{k_{P'(3)}} + \theta_{k_{P'(4)}}) \\
 & + \sum_{P \in \mathcal{S}_3} \sum_{P' \in \mathcal{S}_3} \text{sgn}(P) \text{sgn}(P') [\cos(k_{P(1)} \\
 & - k_{P'(3)} - \theta_{k_{P(1)}} + \theta_{k_{P(2)}} + \theta_{k_{P'(3)}} - \theta_{k_{P'(4)}}) \\
 & + \cos(k_{P(1)} - k_{P'(3)} - \theta_{k_{P(1)}} - \theta_{k_{P(2)}} + \theta_{k_{P'(3)}} \\
 & \left. + \theta_{k_{P'(4)}}) \right]), \quad (24)
 \end{aligned}$$

where P and P' act on $\{1,2\}$ and $\{3,4\}$, respectively.

New quadratic terms are generated by normal ordering the quartic piece. We must then include these with the original terms from H_2 and solve for θ_k self-consistently so that the off-diagonal terms are zero. This requirement may be recast as a self-consistency condition for every k ,

$$\tan(2\theta_k) = \frac{2 \sin(2k) + \frac{2h}{J} \sin(k) + \frac{1}{2N} \sum_q \Theta_2(k, q)}{\Delta + 2 \cos(2k) + \frac{2h}{J} \cos(k) + \frac{1}{N} \sum_q \Theta_1(k, q)}, \quad (25)$$

where we have defined

$$\Theta_1(k, q) = 2f_{(k,q)(-k,-q)} \sin^2(\theta_q) + g_{(k,q,-q)} \sin(2\theta_q), \quad (26)$$

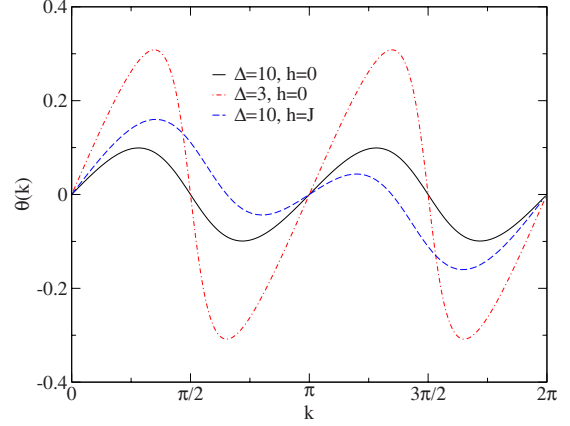


FIG. 1. (Color online) The self-consistent Bogoliubov parameter θ_k for $J=1$. The parameter scales as Δ^{-1} .

$$\Theta_2(k, q) = f_{(k,-k)(q,-q)} \sin(2\theta_q) - 4g_{(k,-k,q)} \sin^2(\theta_q). \quad (27)$$

Clearly the dispersion is also affected by the new quadratic parts becoming

$$\begin{aligned}
 \epsilon_k = & J \left(\left[\frac{\Delta}{2} + \cos(2k) + \frac{h}{J} \cos(k) + \frac{1}{2N} \sum_q \Theta_1(k, q) \right]^2 \right. \\
 & \left. + \left[\sin(2k) + \frac{h}{J} \sin(k) + \frac{1}{4N} \sum_q \Theta_2(k, q) \right]^2 \right)^{1/2}. \quad (28)
 \end{aligned}$$

Evaluating the self-consistency and dispersion relations [Eqs. (25) and (28)] numerically we can compare the gap (i.e., lowest excitation energy) to the mean-field result found by Gómez-Santos.⁴⁰ Summing over 100 sites our results for the physical (two-particle) gap are in excellent agreement. The self-consistent Bogoliubov parameter is plotted in Fig. 1 for a range of parameters. Figures 2 and 3 show that ϵ_k is an excellent approximation to the spinon dispersion. It is also

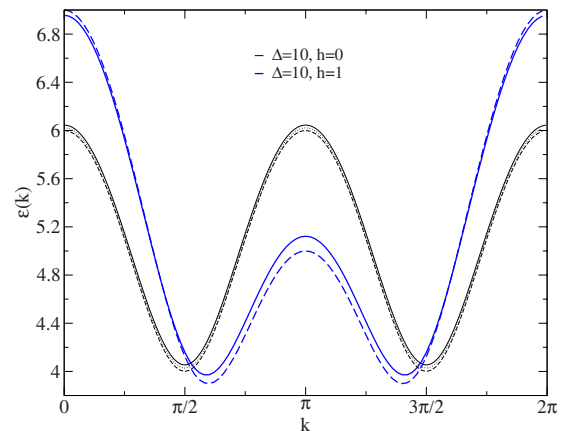


FIG. 2. (Color online) The single-particle dispersion relation, ϵ_k (with $J=1$), for $\Delta=10$. The dispersion calculated with and without self-consistency (solid and dashed curves, respectively) and the exact spinon dispersion (Refs. 26 and 28) (dotted curves) are shown. The spinon result is not available in the case of a finite transverse field. For $h=0$ the dispersion is nearly sinusoidal. Note the functions are π periodic for $h=0$ and 2π periodic otherwise.

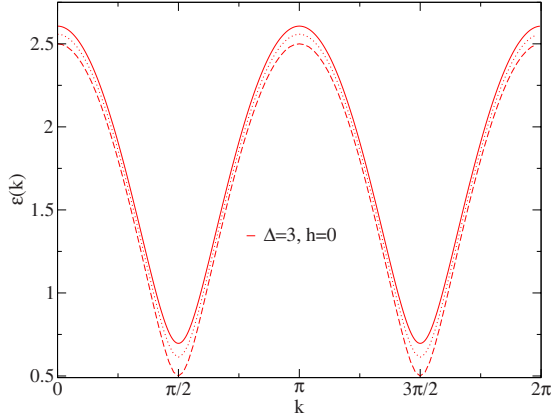


FIG. 3. (Color online) The single-particle dispersion relation, ϵ_k (with $J=1$), for $\Delta=3$. The dispersion calculated with and without self-consistency (solid and dashed curves, respectively) and the exact spinon dispersion (Refs. 26 and 28) (dotted curves) are shown.

apparent that use of a self-consistent Bogoliubov parameter is a small effect on the level of the dispersion, except in the presence of a transverse field.

It is worth emphasizing that the fermions that feature in the diagonalized quadratic Hamiltonian, Eq. (16), are not the same as the spinons of the exact treatment.^{26–28} Here fermion number is not conserved by the interaction vertices. In contrast spinon number is conserved by the exact solution. Instead the fermions described by α_k^\dagger should be viewed as propagating domain walls.

3. Properties of the eigenstates

Previously it has been suggested that the fundamental excitations of Heisenberg-Ising chains are chiral.¹³ We now make some remarks on this possibility, in light of our results. The relevant chiral operator, C_x , is defined as

$$C_x = \hat{x} \cdot \sum_n \mathbf{S}_n \times \mathbf{S}_{n+1} = \sum_n S_n^y S_{n+1}^z - S_n^z S_{n+1}^y. \quad (29)$$

For chirality to be a good quantum number for the XXZ chain, C_x must commute with the Hamiltonian. We find

$$[H, C_x] = \sum_n i(S_{n-1}^x - S_n^x + S_{n+1}^x - S_{n+2}^x)(S_n^y S_{n+1}^y + S_n^z S_{n+1}^z), \quad (30)$$

which is an $\mathcal{O}(1)$ contribution. *A priori*, this demonstrates that at least one eigenstate of the Hamiltonian is not an eigenstate of C_x . However it is possible to show that spinon states are generally not chirality eigenstates. First we write the commutator in the fermionic basis

$$[H, C_x] = -\frac{i}{4} \sum_n \left(c_n^\dagger c_n - \frac{M_{n-1, n+1}}{2} + c_n^\dagger c_n M_{n-1, n+1} \right) \times (M_{n-2, n-1} - M_{n-1, n} + M_{n, n+1} - M_{n+1, n+2}), \quad (31)$$

where we have defined

$$M_{n, n+1} = c_n^\dagger c_{n+1}^\dagger + c_n c_{n+1} - c_n^\dagger c_{n+1} - c_n c_{n+1}^\dagger. \quad (32)$$

As written, Eq. (31) contains only terms quartic and sextic in the creation and annihilation operators. However once Fourier transformed, rewritten in the Bogoliubov basis (α_k^\dagger), and normal ordered, quadratic terms will be generated. A true (one-spinon) excitation of the system, $|\Psi\rangle$, involves a superposition of domain walls created by the α_k^\dagger operators. Schematically

$$|\Psi\rangle = \sum_{i=1}^N \prod_{k_1, \dots, k_i} l_i(k_1, \dots, k_i) \Delta^{1-i} \alpha_{k_i}^\dagger |0\rangle. \quad (33)$$

where the $l_i(k_1, \dots, k_i)$ are c -number functions of the momenta and we have written the small expansion parameter Δ^{1-i} explicitly. It has been shown that at lowest order the excitations are eigenstates of the chirality operator.¹³ However from Eqs. (31) and (33) we see that the expectation $\langle \Psi | [H, C_x] | \Psi \rangle$ will generally not be zero, instead having a finite contribution at lower orders in Δ^{-1} . As $\Delta \rightarrow \infty$ these contributions vanish and at the Ising point the excitations can be chosen as chirality eigenstates.

IV. DYNAMICAL RESPONSE

The quantity of interest for inelastic neutron scattering is the dynamical structure factor $S^{ab}(\omega, Q)$ given by

$$S^{ab}(\omega, Q) = \frac{1}{N} \int_{-\infty}^{\infty} \frac{dt}{2\pi} \sum_{l, l'} e^{i\omega t} e^{-iQ(l-l')} \langle S_l^a(t) S_{l'}^b \rangle. \quad (34)$$

Here $S_l^a = \frac{1}{2} \sigma_l^a$ is the a component of the spin operator at site l . The structure factor is related to the retarded dynamical susceptibility $\chi_R^{ab}(\omega, Q)$,

$$S^{ab}(\omega, Q) = -\frac{1}{\pi} \frac{1}{1 - e^{-\beta\omega}} \text{Im}[\chi_R^{ab}(\omega, Q)], \quad (35)$$

where

$$\chi_R^{ab}(\omega, Q) = \int_0^\beta d\tau e^{i\omega_n \tau} \chi^{ab}(\tau, Q) \Big|_{\omega_n \rightarrow \eta - i\omega},$$

$$\chi^{ab}(\tau, Q) = -\frac{1}{N} \sum_{l, l'} e^{-iQ(l-l')} \langle T_\tau S_l^a(\tau) S_{l'}^b \rangle. \quad (36)$$

Here we have introduced the Matsubara formalism and the expectation implies a thermal trace $\langle \dots \rangle = Z^{-1} \sum_m \langle m | e^{-\beta H} \dots | m \rangle$.

Following the discussion in Sec. I it is apparent that for $h=0$, $\chi^{ab}(\omega, Q)$ and hence $S^{ab}(\omega, Q)$ will be diagonal in the indices a, b but that this is no longer the case for $h>0$, in agreement with experiment.¹³

A. Dynamical structure factor in the fermionic representation

As previously discussed, the Jordan-Wigner transformation introduces nonlocal “strings” which make calculating χ^{zz} complicated. We instead focus our attention on the transverse susceptibility, χ^{xx} .

First the required spin operator must be written in terms of the new fermionic operators

$$\sigma_Q^x = \frac{1}{\sqrt{N}} \sum_k e^{i(Q/2)} [2 \cos(k - \theta_k - \theta_{k+Q} + Q/2) \alpha_k^\dagger \alpha_{k+Q} - i \sin(k - \theta_k - \theta_{k+Q} + Q/2) (\alpha_k^\dagger \alpha_{-k-Q}^\dagger - \alpha_{-k} \alpha_{k+Q})]. \quad (37)$$

We will use Eq. (37) to evaluate the time-ordered dynamical susceptibility

$$\chi^{xx}(\tau, Q) = -\frac{1}{4} \langle T_\tau \sigma_Q^x(\tau) \sigma_{-Q}^x \rangle. \quad (38)$$

As we aim to calculate Eq. (38) in perturbation theory in H_4 we now switch to the interaction picture. In order to simplify the perturbative calculation of χ^{xx} it is useful to express Eq. (38) in terms of a 3×3 matrix $\Pi_{\beta\gamma}(\tau, Q|k, k')$ (the matrix indices take values $\beta, \gamma = 1, 2, 3$) as follows:

$$\chi^{xx}(\tau, Q) = \frac{1}{N^2} \sum_{k, k'} L_\beta(k) \Pi_{\beta\gamma}(\tau, Q|k, k') L_\gamma^\dagger(k'), \quad (39)$$

where

$$L_\beta(k) = \begin{bmatrix} \frac{i}{2} \sin(\gamma_k) & \cos(\gamma_k) & -\frac{i}{2} \sin(\gamma_k) \end{bmatrix}_\beta, \quad (40)$$

$$\gamma_k = k + Q/2 - \theta_k - \theta_{k+Q}, \quad (41)$$

and the 3×3 matrix $\Pi_{\beta\gamma}(\tau, Q|k, k')$ is given by

$$\Pi_{\beta\gamma}(\tau, Q|k, q) = -\langle T_\tau X_{\beta\beta}(\tau, Q|k) X_{\gamma\gamma}^\dagger(0, Q|q) U(\beta) \rangle, \quad (42)$$

$$X_{\beta\nu}(\tau, Q|k) = \begin{pmatrix} \alpha_{-k} \alpha_{k+Q} & 0 & 0 \\ 0 & \alpha_k^\dagger \alpha_{k+Q} & 0 \\ 0 & 0 & \alpha_k^\dagger \alpha_{-k-Q}^\dagger \end{pmatrix}_{\beta\nu}. \quad (43)$$

The imaginary time-evolution operator in the interaction picture is

$$U(\tau) = T_\tau \exp \left[-\int_0^\tau d\tau_1 H_4(\tau_1) \right]. \quad (44)$$

The Fourier transform of the matrix Π is given by

$$\Pi(i\omega_n, Q|k, q) = \int_0^\beta d\tau e^{i\omega_n \tau} \Pi(\tau, Q|k, q). \quad (45)$$

B. Zeroth order

At zeroth order in perturbation theory we replace $U(\beta)$ in Eq. (42) by 1. All off-diagonal elements then vanish and we find ($\omega_{nm} = \omega_n - \omega_m$),

$$\begin{aligned} \Pi_{11}^0(i\omega_n, Q|k, q) &= \frac{1}{\beta} \sum_{i\omega_m} G_0(i\omega_m, k+Q) G_0(i\omega_m, -k) [\delta_{k,-q-Q} \\ &\quad - \delta_{k,q}] = \frac{n_k + n_{k+Q} - 1}{i\omega_n - \epsilon_k - \epsilon_{k+Q}} [\delta_{k,-q-Q} - \delta_{k,q}], \end{aligned} \quad (46)$$

$$\begin{aligned} \Pi_{22}^0(i\omega_n, Q|k, q) &= \frac{1}{\beta} \sum_{i\omega_m} G_0(i\omega_m, k+Q) G_0(-i\omega_m, k) \delta_{k,q} \\ &= \frac{n_k - n_{k+Q}}{i\omega_n + \epsilon_k - \epsilon_{k+Q}} \delta_{k,q}, \end{aligned} \quad (47)$$

$$\begin{aligned} \Pi_{33}^0(i\omega_n, Q|k, q) &= \frac{1}{\beta} \sum_{i\omega_m} G_0(-i\omega_m, -k-Q) G_0(-i\omega_m, k) \\ &\quad \times [\delta_{k,-q-Q} - \delta_{k,q}] = \frac{n_k + n_{k+Q} - 1}{i\omega_n + \epsilon_k + \epsilon_{k+Q}} [\delta_{k,q} \\ &\quad - \delta_{k,-q-Q}]. \end{aligned} \quad (48)$$

Here $n_k = 1/(e^{\beta\epsilon_k} + 1)$ and the bare Green's function is given by

$$G_0(ik_n, k) = \frac{1}{ik_n - \epsilon_k}. \quad (49)$$

The dynamical susceptibility at zeroth order in perturbation theory is then obtained by substituting the matrix Π^0 into Eq. (39) and carrying out the momentum sums. Taking the thermodynamic limit and analytically continuing to real frequencies, $i\omega_n \rightarrow \omega + i\eta$, we arrive at the following expression for the zeroth-order retarded susceptibility:

$$\begin{aligned} \chi_{R,0}^{xx}(\omega, Q) &= -\int_{-\pi}^{\pi} \frac{dk}{8\pi} \left[\{1 - \cos[2k + Q - 2(\theta_k + \theta_{k+Q})]\} \right. \\ &\quad \times \left(\frac{n_k + n_{k+Q} - 1}{\omega + i\eta - \epsilon_k - \epsilon_{k+Q}} + \frac{1 - n_k - n_{k+Q}}{\omega + i\eta + \epsilon_k + \epsilon_{k+Q}} \right) \\ &\quad - 2\{1 + \cos[2k + Q - 2(\theta_k \\ &\quad \left. + \theta_{k+Q})]\} \frac{n_{k+Q} - n_k}{\omega + i\eta - \epsilon_k + \epsilon_{k+Q}} \right]. \end{aligned} \quad (50)$$

The remaining k integral cannot be carried out analytically in general as the Bogoliubov parameters θ_k need to be determined self-consistently and are therefore only known implicitly. However, in the limit $\Delta \rightarrow \infty$ the integral can be taken and simple expressions for $\chi_{R,0}^{xx}(\omega, Q)$ may be obtained.

In order to evaluate the susceptibility further we take $h = 0$ and expand ϵ_k as a series in $1/\Delta$. This gives

$$\epsilon_k = \frac{J\Delta}{2} + J \cos(2k) + \frac{J}{\Delta} \sin(2k) + \dots, \quad (51)$$

$$\epsilon_{k+Q} + \epsilon_k = J[\Delta + 2 \cos(2k + Q) \cos(Q)] + \dots, \quad (52)$$

$$\epsilon_{k+Q} - \epsilon_k = -2J \sin(2k + Q) \sin(Q) + \dots. \quad (53)$$

We see that poles occur at

$$\omega = 2J \sin(2k_0 + Q) \sin(Q), \quad (54)$$

$$\omega = J[\Delta + 2 \cos(2k_- + Q) \cos(Q)], \quad (55)$$

$$\omega = -J[\Delta + 2 \cos(2k_+ + Q) \cos(Q)]. \quad (56)$$

The contribution from θ_k only enters at $O(1/\Delta)$ so we neglect it. We wish to take the imaginary part of the retarded suscep-

tibility as this is proportional to the dynamical structure factor. Defining

$$P(\omega, E) = \Theta(|E| + \omega)\Theta(|E| - \omega) = \begin{cases} 0 & \text{if } |\omega| > |E| \\ 1 & \text{if } |\omega| \leq |E|, \end{cases} \quad (57)$$

where the Θ 's are Heaviside step functions, we find

$$\begin{aligned} -\text{Im } \chi_{R,0}^{\text{xx}}(Q, \omega) & \\ \approx [1 + \cos(2k_0 + Q)] & \frac{(n_{k_0+Q} - n_{k_0})P[\omega, 2J \sin(Q)]}{16J|\cos(2k_0 + Q)\sin(Q)|} \\ - \frac{1}{2}[1 - \cos(2k_+ + Q)] & \frac{(n_{k_++Q} + n_{k_+} - 1)}{16J|\sin(2k_+ + Q)\cos(Q)|} \\ \times P[\omega + \Delta J, 2J \cos(Q)] & \end{aligned}$$

$$\begin{aligned} + \frac{1}{2}[1 - \cos(2k_- + Q)] & \frac{(n_{k_-+Q} + n_{k_-} - 1)}{16J|\sin(2k_- + Q)\cos(Q)|} \\ \times P[\omega - \Delta J, 2J \cos(Q)], & \quad (58) \end{aligned}$$

with

$$2k_0 + Q = \arcsin\left(\frac{\omega}{2J \sin(Q)}\right), \quad (59)$$

$$2k_+ + Q = \arccos\left[-\frac{1}{2 \cos(Q)}\left(\frac{\omega}{J} + \Delta\right)\right], \quad (60)$$

$$2k_- + Q = \arccos\left[\frac{1}{2 \cos(Q)}\left(\frac{\omega}{J} - \Delta\right)\right]. \quad (61)$$

Using the expansion of ϵ_k one can also show that at next to leading order

$$\begin{aligned} n_{k_0+Q} - n_{k_0} &= \frac{\sinh\left(\frac{1}{2}\beta\omega\right)P[\omega, 2J \sin(Q)]}{\cosh\left(\frac{1}{2}\beta\omega\right) + \cosh\left(\frac{\beta}{2}J\Delta - \frac{\beta}{2}\cot(Q)\{[2J \sin(Q)]^2 - \omega^2\}^{1/2}\right)}, \\ n_{k_++Q} + n_{k_+} - 1 &= -\frac{\cosh\left(\frac{1}{2}\beta\omega\right)P[\omega \pm J\Delta, 2J \cos(Q)]}{\cosh\left(\frac{1}{2}\beta\omega\right) + \cosh\left(\frac{\beta}{2}\tan(Q)\{[2J \cos(Q)]^2 - (\omega \pm J\Delta)^2\}^{1/2}\right)}. \end{aligned} \quad (62)$$

Inserting these relations into the full expression yields

$$\begin{aligned} -\text{Im } \chi_{R,0}^{\text{xx}}(Q, \omega) &\approx \frac{1}{8} \left[\frac{1}{\{[2J \sin(Q)]^2 - \omega^2\}^{1/2}} - \frac{1}{2J \sin(Q)} \right] \frac{\sinh\left(\frac{1}{2}\beta\omega\right)P[\omega, 2J \sin(Q)]}{\cosh\left(\frac{1}{2}\beta\omega\right) + \cosh\left(\frac{\beta}{2}J\Delta - \frac{\beta}{2}\cot(Q)\{[2J \sin(Q)]^2 - \omega^2\}^{1/2}\right)} \\ &+ \frac{1}{32J \cos(Q)} \left[\frac{2J \cos(Q) + (\omega + J\Delta)}{2J \cos(Q) - (\omega + J\Delta)} \right]^{1/2} \frac{\cosh\left(\frac{1}{2}\beta\omega\right)P[\omega + J\Delta, J \cos(Q)]}{\cosh\left(\frac{1}{2}\beta\omega\right) + \cosh\left(\frac{\beta}{2}\tan(Q)\{[2J \cos(Q)]^2 - (\omega + J\Delta)^2\}^{1/2}\right)} \\ &- \frac{1}{32J \cos(Q)} \left[\frac{2J \cos(Q) - (\omega - J\Delta)}{2J \cos(Q) + (\omega - J\Delta)} \right]^{1/2} \frac{\cosh\left(\frac{1}{2}\beta\omega\right)P[\omega - J\Delta, 2J \cos(Q)]}{\cosh\left(\frac{1}{2}\beta\omega\right) + \cosh\left(\frac{\beta}{2}\tan(Q)\{[2J \cos(Q)]^2 - (\omega - J\Delta)^2\}^{1/2}\right)}. \end{aligned} \quad (63)$$

This analysis shows that, at zeroth order, the response diverges as an inverse square root both for $\omega = \pm[\Delta J - 2J \cos(Q)]$ and $\omega = \pm 2J \sin(Q)$. These divergences are associated with the gapped two-spinon response and the thermally activated Villain mode, respectively. In fact these expressions bear some resemblance to results for the XY chain.^{21,43} This is not surprising as to zeroth order the transverse correlator probes the dynamics of a pair of free fermions, as does χ^{zz} for the XY chain.

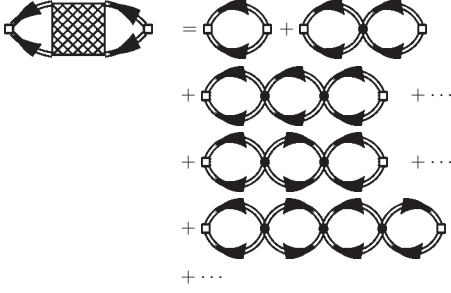


FIG. 4. Bubble summation for one contribution to the dynamical susceptibility matrix $\chi^{\alpha\alpha}(i\omega_n, Q)$. Thick lines indicate that the single-particle propagators may be resummed to include self-energy corrections.

C. First-order perturbation theory

At first order two classes of contributions appear, which may be distinguished by considering their diagrammatic representation. As we have already seen, the three zeroth-order diagrams take the form of bubbles. The first class of diagrams in first order consists of two bubbles connected by an interaction vertex. The second class of diagrams consists of a single bubble with a self-energy insertion. We detail these contributions in Appendix B. An important feature is that several of the first-order contributions have stronger singularities as functions of the external frequency and momentum than the zeroth-order results. This indicates that it is necessary for the expansion to be resummed before useful physical results can be extracted.

V. BUBBLE SUMMATION

We have shown that at zeroth order the susceptibility diverges for certain ω and Q and that this is matched by stronger divergences in some of the first-order terms (see Appendix B). Moreover, it is clear from the first-order calculation that higher orders in perturbation theory will exhibit stronger and stronger divergences. In order to get physically meaningful results we therefore should sum the most divergent classes of diagrams. In the case at hand, the complicated momenta dependence of the vertices and the self-consistent Bogoliubov transformation makes the determination of the most divergent contributions an impossible task. Instead we resum just the connected bubble diagrams and justify our choice by comparing results to the exact $T=0$ calculation. We explain how to incorporate self-energy corrections in Sec. V D.

A. Random-phase approximation–like scheme

The random-phase approximation (RPA) scheme consists of carrying out bubble sums of the type shown in Fig. 4. To carry out these summations is nontrivial as the lines in the internal bubbles can take any orientation and the momentum dependence of the vertices is very complicated. In order to proceed we organize the interaction vertices into a 3×3 matrix

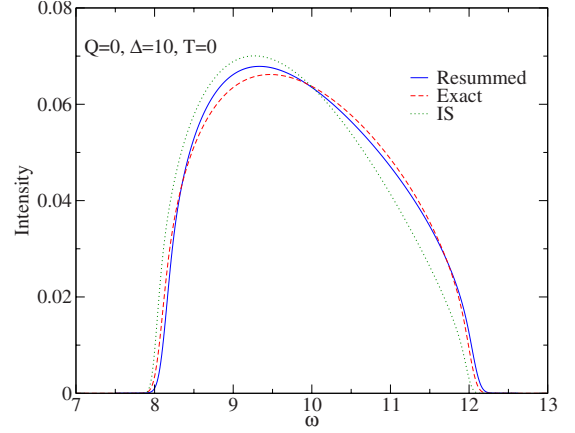


FIG. 5. (Color online) The dynamical structure factor as found by resummation, the exact result (Refs. 26 and 28), and the calculation of Ishimura and Shiba (Ref. 24) (IS) at $T=0$, $Q=0$, and $\Delta=10$. In all cases the curves are convolved with a Gaussian in frequency space of full width at half maximum 0.12.

$$V_{11}(Q|k, q) = V_2(k + Q, -k, q, -q - Q),$$

$$V_{12}(Q|k, q) = -3V_1(q + Q, -q, k, -k - Q),$$

$$V_{13}(Q|k, q) = 6V_0(k + Q, -k, q, -q - Q),$$

$$V_{21}(Q|k, q) = 3V_1(k + Q, -k, q, -q - Q),$$

$$V_{22}(Q|k, q) = -4V_2(k + Q, q, -k, -q - Q),$$

$$V_{23}(Q|k, q) = -3V_1(k, q + Q, -q, -k - Q),$$

$$V_{31}(Q|k, q) = 6V_0(q + Q, -q, k, -k - Q),$$

$$V_{32}(Q|k, q) = 3V_1(q, k + Q, -k, -q - Q),$$

$$V_{33}(Q|k, q) = V_2(q, -q - Q, k + Q, -k). \quad (64)$$

As is shown in Appendix C, in the thermodynamic limit the RPA-like bubble summation without taking into account self-energy corrections results in an integral equation of the form

$$\begin{aligned} \Pi_{\alpha\beta}^{\text{RPA}}(i\omega_n, Q|k, k') &= \Pi_{\alpha\beta}^0(i\omega_n, Q|k, k') \\ &+ \int \frac{dq}{2\pi} K_{\alpha\gamma}(i\omega_n, Q|k, q) \Pi_{\gamma\beta}^{\text{RPA}}(i\omega_n, Q|q, k'), \end{aligned} \quad (65)$$

where the kernel K is defined as the infinite volume limit of

$$K_{\alpha\beta}(i\omega_n, Q|k, q) = \sum_{k'} \Pi_{\alpha\gamma}^0(i\omega_n, Q|k, k') V_{\gamma\beta}(Q|k', q). \quad (66)$$

Defining a convolution $*$ by

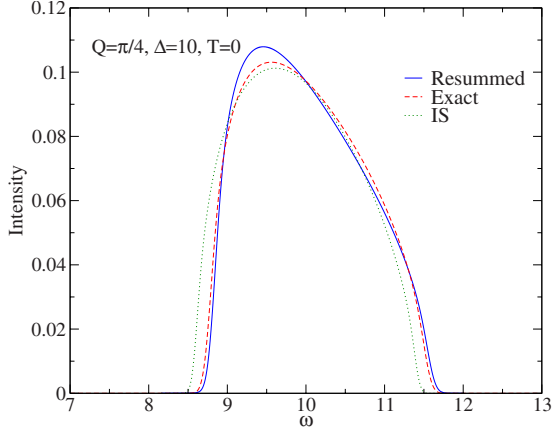


FIG. 6. (Color online) The dynamical structure factor as found by resummation, the exact result (Refs. 26 and 28), and the calculation of IS (Ref. 24) at $T=0$, $Q=\pi/4$, and $\Delta=10$. In all cases the curves are convolved with a Gaussian in frequency space of full width at half maximum 0.12.

$$(X * Y)_{\alpha\beta}(i\omega_n, Q, k, k') \equiv \int_{-\pi}^{\pi} \frac{dq}{2\pi} X_{\alpha\gamma}(i\omega_n, Q|k, q) Y_{\gamma\beta}(i\omega_n, Q|q, k'), \quad (67)$$

this can be rewritten as

$$(\mathbf{I} - \mathbf{K}) * \mathbf{\Pi}^{\text{RPA}} = \mathbf{\Pi}^0. \quad (68)$$

The integral Eq. (68) is then readily solved

$$\mathbf{\Pi}^{\text{RPA}} = (\mathbf{I} - \mathbf{K})^{-1} * \mathbf{\Pi}^0. \quad (69)$$

After analytic continuation to real frequencies $i\omega_n \rightarrow \omega + i\eta$ the quantity of interest is calculated as

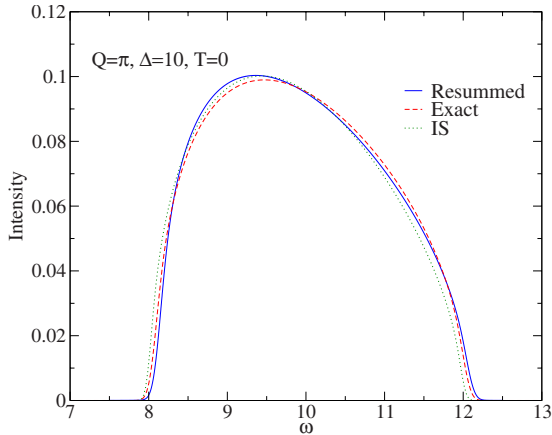


FIG. 7. (Color online) The dynamical structure factor as found by resummation, the exact result (Refs. 26 and 28), and the calculation of IS (Ref. 24) at $T=0$, $Q=\pi$, and $\Delta=10$. In all cases the curves are convolved with a Gaussian in frequency space of full width at half maximum 0.12.

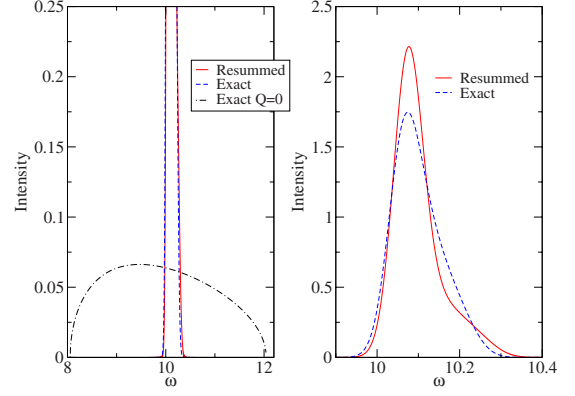


FIG. 8. (Color online) A comparison of our calculation and the exact result (Refs. 26 and 28) for $Q=\pi/2$ at $T=0$ and $\Delta=10$. Left panel: $\pi/2$ curves convolved with a Gaussian (width 0.08) plotted with the exact result at $Q=0$, in order to demonstrate the scale. Right panel: the same $\pi/2$ curves but plotted at a different scale. At $Q=\pi/2$ the result of Ishimura and Shiba is undefined as the denominator goes to zero (Ref. 24).

$$\int_{-\pi}^{\pi} \frac{dkdq}{(2\pi)^2} L_{\alpha}(k) \mathbf{\Pi}_{\alpha\beta}^{\text{RPA}}(\omega + i\eta, Q|k, q) L_{\beta}^{\dagger}(q). \quad (70)$$

In practice the solution of the integral equation discussed above is reduced to a simple matrix inversion problem. We discretize all momentum integrals in terms of sums over $N=400$ points. We find that this value is large enough to make discretization effects negligible. We set $J=1$ and the regulator $\eta=10^{-3}$. The discretized representation of $\mathbf{I} - \mathbf{\Pi}^0 * \mathbf{V}$ (which is a matrix both in momentum space as well as in the 3×3 matrix space labeled by Greek indices) may be found using standard linear algebra routines. The dynamical structure factor is then evaluated at 24 000 points in frequency space. Using a finite system size results in a finite number of poles in the susceptibility (36). In turn, because η is finite, the calculated structure factor will be composed of a number

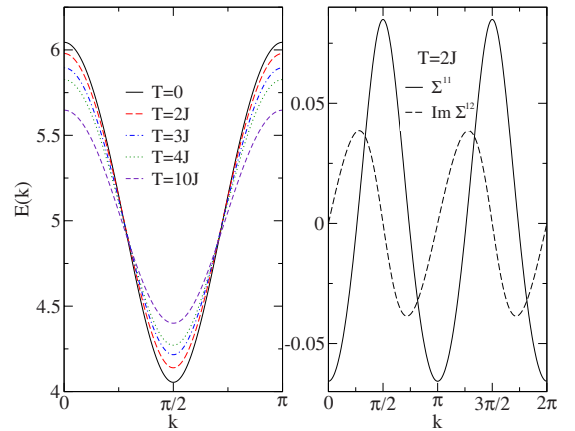


FIG. 9. (Color online) The dispersion E_k , including tadpole self-energy corrections for $\Delta=10$. Left panel shows the gradual narrowing of the bandwidth with temperature. At this scale the dispersion for $T=J$ is indistinguishable from that for $T=0$. Right panel shows the two distinct elements of the self-energy matrix, Σ_{sp} at $T=2J$.

$\sim N$ of Lorentzian peaks of width η . Finally we convolve this result with a suitable Gaussian.

B. Comparison to exact results for $T=0$

Given the uncontrolled nature of our bubble summation it is essential to compare it to exact results at zero temperature^{26,28} in order to assess its quality. In Figs. 5–8 we plot our results against the exact results for the dynamical structure factor for $\Delta=10$, $T=0$, and several momenta. We also include for comparison an earlier result for the DSF due to Ishimura and Shiba.²⁴ We see that for $\Delta=10$, $T=0$, and at most wave vectors the resummation is a highly accurate approximation. This suggests that the diagrams we have selected account for most of the spectral weight at low temperature. It is known from the exact result^{26,28} that the gapped response diverges along its lower energy threshold, in a region of momentum centered about $\pi/2$ (the size of which increases as $\Delta \rightarrow 1$). Correspondingly the resummation is less accurate near $\pi/2$, although there is still qualitative agreement (Fig. 8). For larger values of Δ our approximation becomes even better.

C. Analytical resummation for $T=0$

It is possible and instructive to evaluate the resummation exactly in the limit $T=0$, $\Delta \rightarrow \infty$. At zeroth order, positive frequencies, and $T=0$, the only nonzero diagram is the particle-particle propagation bubble. This diagram leads to a response in the region $\omega \sim \Delta J$. As $T \rightarrow 0$ the thermal occupation factors vanish and by expanding in $1/\Delta$ we find

$$\theta_k = \mathcal{O}(\Delta^{-1}), \tag{71}$$

so that we can neglect the Bogoliubov phases. The diagram then reduces to

$$\int \frac{dk}{4\pi} \frac{\sin^2(k+Q/2)}{i\omega_n - \epsilon_k - \epsilon_{k+Q}} = A(i\omega_n, Q). \tag{72}$$

Using the approximation

$$\epsilon_k + \epsilon_{k+Q} \approx \Delta J + 2J \cos(Q) \cos(2k+Q),$$

we have

$$\begin{aligned} A(i\omega_n, Q) &= \int_{-\pi}^{\pi} \frac{dk}{4\pi} \frac{\sin^2(k+Q/2)}{i\omega_n - \epsilon_k - \epsilon_{k+Q}} \\ &= \frac{1}{4J \cos(Q)} \int_0^{\pi} \frac{dk}{2\pi} \frac{1 - \cos(2k+Q)}{\tilde{\omega} - \cos(2k+Q)} \end{aligned}$$

and $\tilde{\omega} = \frac{i\omega_n - \Delta J}{2J \cos(Q)}$. The remaining integral can be taken by standard contour integration methods and analytic continuation to real frequencies is then straightforward. With the approximations made here the vertex V_2 takes a particularly simple form and resummation amounts to the geometric series

$$\begin{aligned} -\text{Im}[\chi^{xx}(\omega, Q)] &= -\text{Im}[A(\omega, Q) + 4J \cos(Q)A(\omega, Q)^2 \\ &\quad + (4J)^2 \cos^2(Q)A(\omega, Q)^3 + \dots] \\ &= -\text{Im}\left[\frac{A(\omega, Q)}{1 - 4J \cos(Q)A(\omega, Q)} \right]. \end{aligned} \tag{73}$$

Finally the $T=0$ result, to lowest order in Δ , is

$$-\text{Im}[\chi^{xx}(\omega, Q)] = \begin{cases} \frac{\sqrt{[2J \cos(Q)]^2 - (\omega - \Delta J)^2}}{8J^2 \cos^2(Q)} & |\omega - \Delta J| \leq |2J \cos(Q)| \\ 0 & \text{otherwise.} \end{cases} \tag{74}$$

Ishimura and Shiba calculated the DSF at $T=0$ using a method based on perturbation theory combined with a Lehmann representation.²⁴ The expression obtained here (74) agrees to lowest order with their result.

D. One-loop self-energy corrections

As they stand, the first-order tadpole contributions, Eqs. (B10)–(B16), cannot be incorporated into the RPA. This is because they contain divergences which are not resummed according to the scheme above. Instead we must first calculate a new single-particle Green’s function using a Dyson equation to resum the tadpole self-energy corrections. This Green’s function is then used to calculate a new bubble diagram.

Including the tadpole corrections generates anomalous propagators at higher orders. These are most efficiently taken into account by formulating the propagator as a matrix

$$g(i\omega_n, k) = - \int_0^{\beta} d\tau e^{i\omega_n \tau} g(\tau, k),$$

$$g(\tau, k) = \left\langle T_{\tau} \begin{pmatrix} \alpha_k(\tau) \alpha_k^{\dagger}(0) & \alpha_k(\tau) \alpha_{-k}(0) \\ \alpha_{-k}^{\dagger}(\tau) \alpha_k^{\dagger}(0) & \alpha_{-k}^{\dagger}(\tau) \alpha_{-k}(0) \end{pmatrix} U(\beta, 0) \right\rangle. \tag{75}$$

At zeroth order the result is

$$g_0(i\omega_n, k) = \begin{pmatrix} G_0(i\omega_n, k) & 0 \\ 0 & -G_0(-i\omega_n, -k) \end{pmatrix}. \tag{76}$$

The single-particle self-energy is defined by the Dyson equation

$$\mathbf{g}^{-1}(i\omega_n, k) = \mathbf{g}_0^{-1}(i\omega_n, k) - \mathbf{\Sigma}(i\omega_n, k). \quad (77)$$

If only ‘‘tadpole’’-type diagrams are included the self-energy is, to first order in perturbation theory, frequency independent

$$\mathbf{\Sigma} = \sum_p \frac{n_p}{N} \begin{pmatrix} 4V_2(k, p, -p, -k) & -3V_1(p, -p, k, -k) \\ 3V_1(p, -p, k, -k) & -4V_2(k, p, -p, -k) \end{pmatrix}. \quad (78)$$

The elements of the matrix are $\mathcal{O}(n_k \Delta^0)$ and hence their effects will be most pronounced when the gap is small or the temperature is large.

Using the relations

$$g_0^{11}(i\omega_n, k) = \frac{1}{i\omega_n - \epsilon_k}, \quad (79)$$

$$g_0^{22}(i\omega_n, k) = \frac{1}{i\omega_n + \epsilon_k}, \quad (80)$$

$$\Sigma^{21} = (\Sigma^{12})^* = -\Sigma^{12}, \quad (81)$$

$$\Sigma^{11} = -\Sigma^{22}, \quad (82)$$

one finds that

$$\mathbf{g}(i\omega_n, k) = \frac{1}{(i\omega_n)^2 - (\epsilon_k + \Sigma^{11})^2 - |\Sigma^{12}|^2} \begin{pmatrix} i\omega_n + \epsilon_k + \Sigma^{11} & -\Sigma^{12} \\ \Sigma^{12} & i\omega_n - \epsilon_k - \Sigma^{11} \end{pmatrix}.$$

We rewrite this as

$$g^{11}(i\omega_n, k) = \left(\frac{Z_k^-}{i\omega_n - E_k} + \frac{Z_k^+}{i\omega_n + E_k} \right), \quad (83)$$

$$g^{22}(i\omega_n, k) = \left(\frac{Z_k^-}{i\omega_n + E_k} + \frac{Z_k^+}{i\omega_n - E_k} \right), \quad (84)$$

$$g^{12}(i\omega_n, k) = \lambda_k \left(\frac{1}{i\omega_n + E_k} - \frac{1}{i\omega_n - E_k} \right), \quad (85)$$

$$g^{21}(i\omega_n, k) = -g^{12}(i\omega_n, k), \quad (86)$$

with the definitions

$$E_k = \sqrt{(\epsilon_k + \Sigma^{11})^2 + |\Sigma^{12}|^2}, \quad (87)$$

$$Z_k^\pm = \frac{1}{2} \left(1 \mp \frac{\epsilon_k + \Sigma^{11}}{E_k} \right), \quad \lambda_k = \frac{\Sigma^{12}}{2E_k}. \quad (88)$$

E. Bubble summation with self-energy corrections

The one-loop self-energy corrections to the propagators can be taken into account in the bubble summation for the dynamical susceptibility as follows. We define a 3×3 matrix $\mathbf{\Pi}^S$ by

$$\Pi_{\beta\gamma}^S(\tau, Q|k, q) = -\langle T_\tau X_{\beta\beta}(\tau, Q|k) X_{\gamma\gamma}^\dagger(0, Q|q) U(\beta) \rangle_{1\text{-loop } \Sigma}, \quad (89)$$

where only one-loop self-energy corrections are taken into account. This amounts to calculating the two-point function of X and X^\dagger using the (anomalous) propagators (82). The elements of $\mathbf{\Pi}^S$ are listed in Appendix D. We now follow the same steps as in Appendix C and show that summing all bubble diagrams of the form shown in Fig. 4 gives rise to an

integral equation obtained from Eq. (65) by the replacement $\Pi_{\alpha\beta}^0 \rightarrow \Pi_{\alpha\beta}^S$, i.e.,

$$\begin{aligned} \Pi_{\alpha\beta}^{\text{RPA}}(i\omega_n, Q|k, k') &= \Pi_{\alpha\beta}^S(i\omega_n, Q|k, k') \\ &+ \int \frac{dq}{2\pi} K_{\alpha\gamma}^S(i\omega_n, Q|k, q) \Pi_{\gamma\beta}^{\text{RPA}}(i\omega_n, Q|q, k'), \end{aligned} \quad (90)$$

where the kernel K^S is defined as the infinite volume limit of

$$K_{\alpha\beta}^S(i\omega_n, Q|k, q) = \sum_{k'} \Pi_{\alpha\gamma}^S(i\omega_n, Q|k, k') V_{\gamma\beta}(Q|k', q). \quad (91)$$

At $T=0$ the one-loop corrections to $\mathbf{\Sigma}$ vanish, so that we recover our previous result. On the other hand, for $T>0$, $\mathbf{\Sigma}$ plays an important role, altering the dispersion and shifting the thresholds of the dynamical response (see Fig. 9).

One can also calculate the two-loop corrections to the single-particle propagator but it is not as simple to incorporate them into the RPA. For reference they are included in Appendix E.

VI. RESULTS AND DISCUSSION

We now turn to a discussion of our results at finite temperatures and applied fields. For the perturbative expansion to be valid we require $\Delta \gg 1$. In selecting diagrams to resum we have favored those that are most relevant at low temperatures, i.e., those that feature few thermal occupation factors. The relevant energy scale is the single-particle gap $\sim \Delta J/2$, so we restrict our discussion to temperatures $T < \Delta J/2$. We calculate the transverse dynamical structure factor as described in Sec. V A using the matrix $\mathbf{\Pi}^S$ found in Sec. V D and setting $\Delta=10$ and $J=1$. For $\Delta \gg 1$ the dynamical structure factor (at positive frequency) consists of two pieces: a gapped continuum response occurring at frequencies $\omega \sim \Delta$

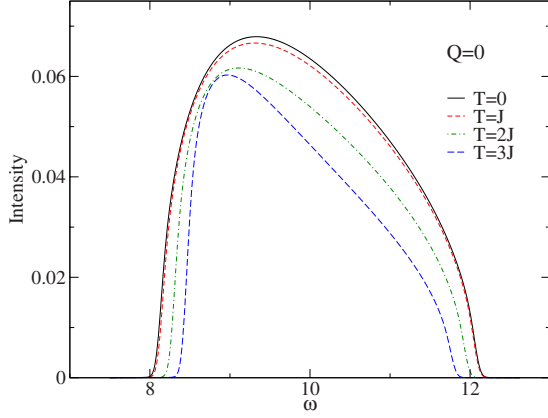


FIG. 10. (Color online) The dynamical structure factor at finite temperature for $\omega \sim \Delta$ and $\Delta=10$ at wave vector $Q=0$.

and a response for $\omega \sim 0$ that is only seen at finite temperature.

On general grounds one expects that at finite temperature the very sharp thresholds seen at $T=0$ should disappear. In our approach the thresholds are still present although they are obfuscated by the necessity of convolving the response with a Gaussian. This is a consequence of the diagrams we have taken into account. We expect this “thermal broadening” to be a small effect that could be taken into account by including certain two-loop diagrams. These two-loop diagrams connect the response to decay channels of higher particle number. We discuss the issue further in Appendix E.

A. Gapped response for $h=0$

We first consider the gapped (interband) response at finite temperatures and for $h=0$. At $T=0$ the transverse DSF is dominated by a two-spinon scattering continuum that occurs at energies around twice the single-particle gap, i.e., $\omega \sim \Delta J$. In Figs. 10–12 we show how the DSF in this regime of energies changes at finite temperature. The most striking feature is a narrowing of the response with increasing temperature. This is in agreement with inelastic neutron-scattering experiments on TiCoCl_3 .¹¹ Another notable feature at $T=0$ is

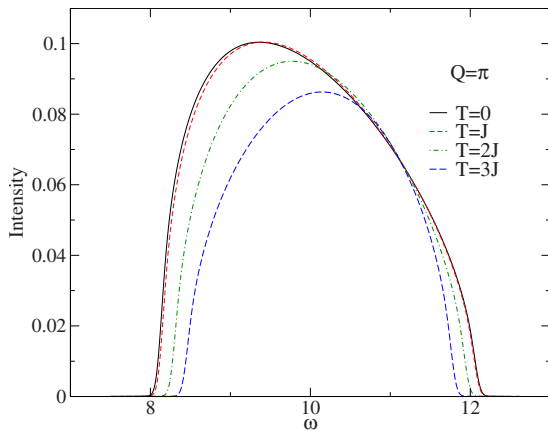


FIG. 11. (Color online) The dynamical structure factor at finite temperature for $\omega \sim \Delta$ and $\Delta=10$ at wave vector $Q=\pi$.

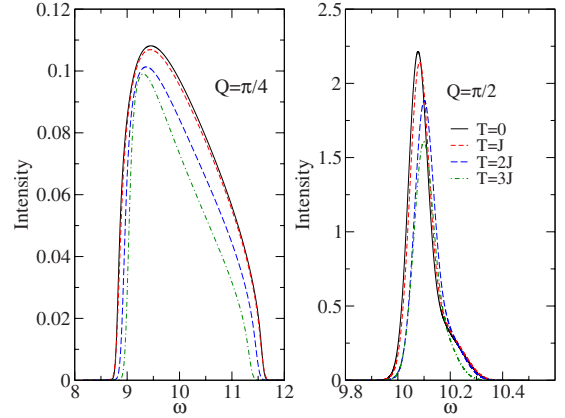


FIG. 12. (Color online) The dynamical structure factor at finite temperature for $\omega \sim \Delta$ and $\Delta=10$ at wave vectors $Q=\pi/4$ and $\pi/2$. Note that the scale of the intensity axes differs dramatically between the two plots.

that the response is not symmetric about $Q=\pi/2$.²⁶ As can be seen in Figs. 5–7 our calculation captures this behavior. Accordingly the response develops asymmetrically with temperature and in a nontrivial way. In particular the maximum of the response for $0 \leq Q < \pi/2$ moves to lower frequencies as temperature increases, but is shifted to higher frequencies for $\pi/2 < Q \leq \pi$.

For all wave vectors the total spectral weight in the gapped region decreases as temperature increases. The thresholds of the response shift as temperature increases due to the thermal dependence of the single-particle dispersion E_k , Eq. (87). This depletion of spectral weight is physically sensible because the excitations are fermionic; as temperature increases more states are thermally occupied and concomitantly there are fewer states for the new pair of fermions to fill.

B. Villain mode for $h=0$

At temperatures greater than zero there is a thermal population of spin excitations. Neutron scattering can then lead to processes that do not change the spinon number of a given microstate, thus giving rise to an intraband response at low energies, $\omega \sim 0$. Dynamics of this kind were first described by Villain for the case of an finite length chain with an odd number of sites.¹⁵ As such processes rely on states being thermally occupied; their contribution to the DSF grows with temperature. The principle feature of the response is a well-defined resonance or “mode” at $\omega=2J \sin(Q)$.^{8,9,15} At lowest order in our calculation the intraband response exhibits a square-root divergence (Sec. IV B). Taking interactions into account by our bubble summation leads to a smoothing of the divergence, which however occurs in a very small region in energy close to the threshold. This means that the zeroth order (especially when convolved with an experimental resolution) is an excellent approximation to the resummed result.

The intraband response is also asymmetric about $Q=\pi/2$ (see Fig. 13). For $0 \leq Q < \pi/2$ the response between

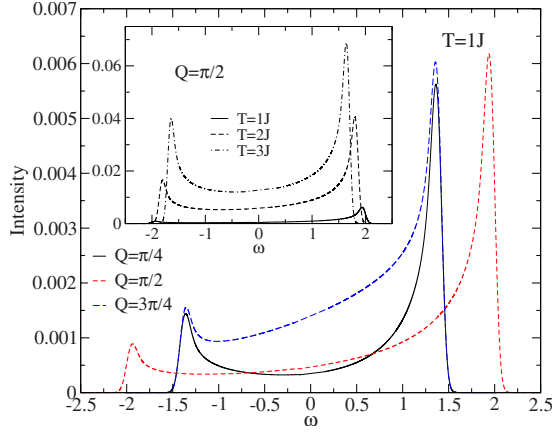


FIG. 13. (Color online) The dynamical structure factor for $\omega \sim 0$ and $\Delta=10$. Main plot: the Villain mode for a range of wave vectors. Inset: the development of the Villain mode at $Q=\pi/2$ with temperature.

the peaks is suppressed relative to that at $Q=\pi/2$. For $\pi/2 < Q \leq \pi$ it is enhanced.

C. Response in a transverse field

The transverse field h only enters the quadratic part of the Hamiltonian (16), hence its influence on the scattering response is through the single-particle dispersion and not the interaction vertices. The first property to take into consideration is that h will have an effect on the excitation gap. As the magnitude of the field h approaches ΔJ the gap collapses and the perturbative expansion is inapplicable. Hence we consider a field small compared to ΔJ . For fields $h \gg \Delta J$ the gap opens again with the chain ferromagnetically ordered. A second important feature to note is that a nonzero h causes the period of E_k to double (see Fig. 1): the maximum at $k=(2n+1)\pi$ is reduced relative to those at $k=2n\pi$. This leads to the double-peaked structure seen at $Q=\pi/2$ in the gapped response (Figs. 14 and 15) and throughout the low energy scattering (Fig. 16). This splitting of the Villain mode peaks was observed by Braun *et al.*¹³

The asymmetry of the response about $Q=\pi/2$ is further increased by the transverse field. In particular, though the exact result at $T=0$ (Refs. 26 and 28) and $\Delta=10$ shows that the energy *thresholds* of the gapped response are very nearly symmetric about $\pi/2$, this is no longer the case in a finite field. Instead the upper threshold near $Q=0$ is pushed to higher energies but is relatively unchanged near $Q=\pi$. We also note that the narrowing in energy of the response near $Q=\pi/2$ is suppressed relative to $h=0$. Asymmetry is also seen in the thresholds of the low energy response (Fig. 16).

VII. COMPARISON TO DIAGONALIZATION OF SHORT CHAINS AT $T > 0$

As we have seen above, at zero temperature our approach gives good agreement with the exact DSF. In order to assess the quality of our approximate DSF at finite temperatures, we have computed the DSF by means of numerical diagonalization of the Hamiltonian on finite periodic chains of up

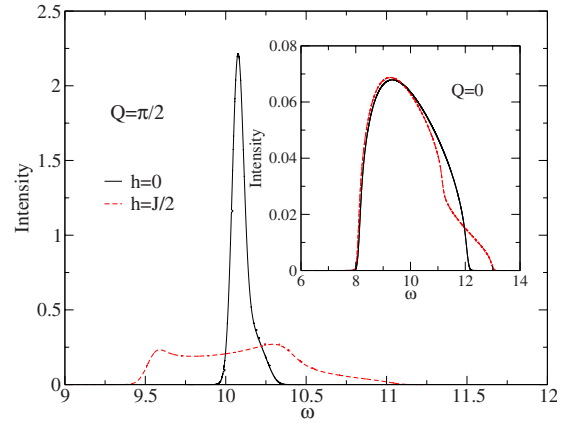


FIG. 14. (Color online) Comparison of the $T=0$ dynamical structure factor for $\Delta=10$ with and without an applied transverse field $h=J/2$. Main panel: the divergent response at $\pi/2$ is split into a much broader two-peaked structure by the application of the field. Inset: the effect of the field at $Q=0$ is only apparent at the upper threshold.

to 16 sites. The dynamical susceptibility (36) is expressed by means of a Lehmann expansion in terms of Hamiltonian eigenstates $|n\rangle$ of energy E_n as

$$\chi^{xx}(\omega, Q) = N \sum_{n,m} \frac{e^{-\beta E_n} - e^{-\beta E_m}}{\omega + i\eta + E_n - E_m} \delta_{Q+p_n, p_m} \langle n | S_0^x | m \rangle \langle m | S_0^x | n \rangle, \quad (92)$$

where the sums are taken over the eigenbasis of H . For a sufficiently small system the eigenstates can be calculated numerically. Due to the exponential increase in the dimension of the Hilbert space with the number of sites the method is restricted to short chains. We consider systems with $N \leq 16$. In order to approximate the thermodynamic spectrum from a finite number of allowed transitions, we take the parameter η in Eq. (92) to be sufficiently large so that the finite sum of Lorentzians in Eq. (92) becomes a smooth function of

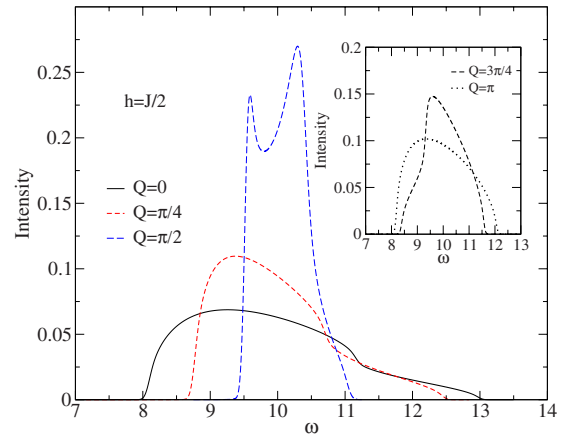


FIG. 15. (Color online) Wave vector dependence of the dynamical structure factor for $\Delta=10$ at $h=J/2$, $T=0$. Main panel shows wave vectors $Q=0$, $\pi/4$, and $\pi/2$. Inset shows plots for $Q=3\pi/4$ and π .

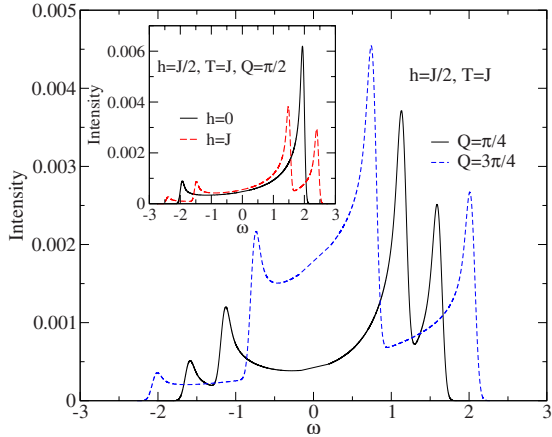


FIG. 16. (Color online) Wave vector dependence of the Villain mode for $\Delta=10$ at $h=J/2$, $T=J$. Main panel shows wave vectors $Q=\pi/4$, $\pi/2$, and $3\pi/4$. Inset shows the response at $Q=\pi/2$ for $h=0$ and $h=J/2$.

(the real part of the) frequency. Clearly this procedure can give a meaningful approximation of the susceptibility in the thermodynamic limit only if η is very small in comparison to the thermal broadening. Hence the method is restricted to sufficiently large temperatures. In order to obtain a measure of the importance of finite-size effects we calculate the DSF for system sizes $N=8, 12$, and 16 . We find that the finite-size effects depend strongly on which region of energy and the momentum we consider.

In Figs. 17–20 we compare the dynamical structure factor calculated for a 16-site chain to the results obtained by our perturbative approach for several values of momentum. For $Q=0, \pi$, and $T=2J$ (Figs. 17 and 18) the agreement of the two methods is good. The difference at very small frequencies is probably due to finite-size effects in the exact diagonalization results. The finite-size effects for the main peak are found to be quite small.

At $Q=\pi/2$ and $T=2J$ (Fig. 19) the agreement of the two methods is less impressive. The disagreement at high fre-

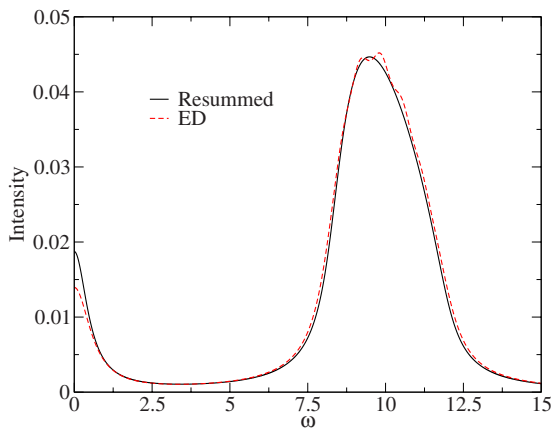


FIG. 17. (Color online) Comparison of the dynamical structure factor obtained from the perturbative approach to exact diagonalization on a 16-site chain with $\eta=0.5J$ for $T=2J$ at momentum $Q=0$. In order to facilitate a comparison the perturbative result has been convolved with a Lorentzian of width η .

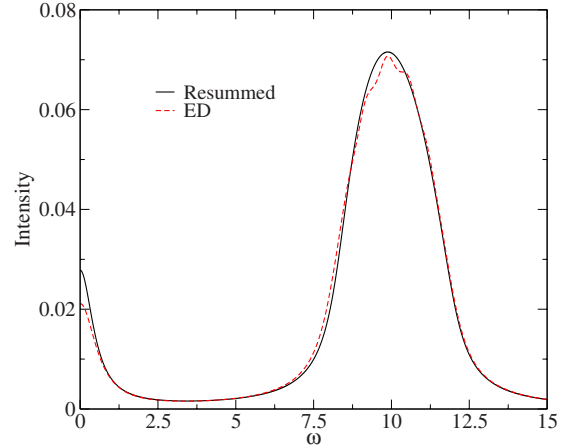


FIG. 18. (Color online) Comparison of the dynamical structure factor obtained from the perturbative approach to exact diagonalization on a 16-site chain with $\eta=0.5J$ for $T=2J$ at momentum $Q=\pi$. In order to facilitate a comparison the perturbative result has been convolved with a Lorentzian of width η .

quencies is likely due to inaccuracy of the bubble summation in our perturbative method (we recall that the agreement of our resummation with the exact result at $T=0$ was worst for $Q=\pi/2$). On the other hand, the exact diagonalization results are found to still suffer from finite-size effects at small frequencies.

VIII. CONCLUSIONS

We have calculated the transverse dynamical structure factor of the XXZ spin chain at finite temperature and applied field. The perturbative method we use is accurate at low temperatures and for large $\Delta \geq 10$. In this case the chain is in the Ising phase and the excitations are descended from propagating domain walls. The scattering response is com-

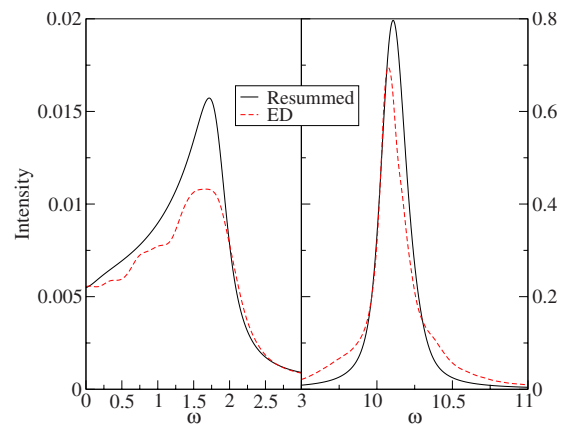


FIG. 19. (Color online) Comparison of the dynamical structure factor obtained from the perturbative approach to exact diagonalization on a 16-site chain for $T=2J$ at momentum $Q=\pi/2$. Left panel: low-frequency response with $\eta=0.2J$. Right panel: high-frequency response with $\eta=0.05J$. In order to facilitate a comparison the perturbative results have been convolved with a Lorentzian of width η .

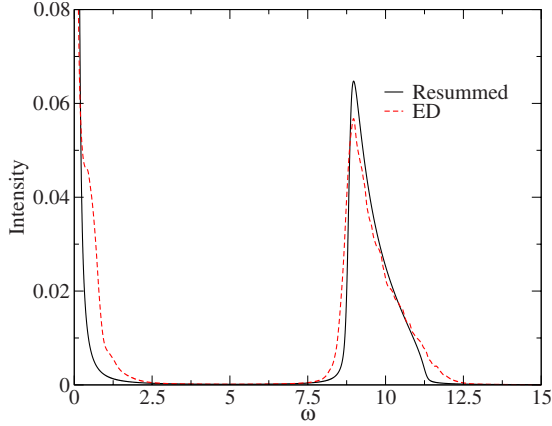


FIG. 20. (Color online) Comparison of the dynamical structure factor obtained from the perturbative approach to exact diagonalization on a 16-site chain with $\eta=0.05J$ for $T=10J$ at momentum $Q=0$. In order to facilitate a comparison the perturbative result has been convolved with a Lorentzian of width η .

posed of two distinct parts for $\Delta \gtrsim 10$, namely, a gapped continuum at $\omega \sim \Delta J$ and the Villain mode at $\omega \sim 0$. Our results pertain to the low temperature and field dependence of both. Our main observations are:

(1) The response associated with the gapped two-spinon continuum at $T=0$ narrows in energy as temperature is increased and loses spectral weight to the emerging low-frequency Villain mode.

(2) The position of the peak (as a function of frequency) of the high-frequency (gapped) continuum at $T > 0$ becomes asymmetric about $Q = \pi/2$ as temperature increases.

(3) The thermally activated response at low frequencies $\omega \sim 0$ is asymmetric about $Q = \pi/2$.

(4) The Villain mode splits into two peaks in a transverse field.

The main advantage of our method compared to previous theoretical approaches lies in the fact that it is not restricted to asymptotically large values of Δ and treats the Villain mode and the gapped response in a unified way, which allows us to determine the ratio of spectral weights between these two features. Our results are in qualitative agreement with inelastic neutron-scattering experiments.^{8,9,11,13} It would be interesting to perform quantitative comparisons with polarized neutron-scattering data.

ACKNOWLEDGMENTS

We are grateful to Alan Tennant for getting us interested in this problem and to Isaac Pérez-Castillo for his collabora-

tion on the early part of this work and for many helpful discussions since. In particular we thank him for providing efficient code to generate the exact solution curves at $T=0$. We thank I. Affleck, S. E. Nagler, and A. M. Tsvelik for useful discussions. This work was supported by the EPSRC under Grant No. EP/D050952/1.

APPENDIX A: DIRECT JORDAN-WIGNER TRANSFORMATION OF THE HAMILTONIAN

We may write the Hamiltonian (1) as $H=H_0+H_1$, where

$$H_0 = \frac{J}{4} \sum_n \Delta \sigma_n^z \sigma_{n+1}^z + \sigma_n^y \sigma_{n+1}^y + \frac{h}{2} \sum_n \sigma_n^x,$$

$$H_1 = \frac{J}{4} \sum_n \sigma_n^x \sigma_{n+1}^x, \quad (\text{A1})$$

where H_0 can then be expressed as a quadratic form in spinless fermions by means of the Jordan-Wigner transformation

$$\sigma_n^x = 2c_n^\dagger c_n - 1,$$

$$\frac{\sigma_n^z - i\sigma_n^y}{2} = -c_n^\dagger \exp\left(-i\pi \sum_{j < n} c_j^\dagger c_j\right). \quad (\text{A2})$$

The full Hamiltonian takes the form

$$H = \sum_n \frac{J}{4} (\Delta + 1) [c_n^\dagger c_{n+1} + \text{H.c.}] + \frac{h - J}{2} c_n^\dagger c_n + \frac{J}{4} \sum_n (\Delta - 1) [c_n^\dagger c_{n+1}^\dagger + \text{H.c.}] + \frac{J}{4} \sum_n c_n^\dagger c_n c_{n+1}^\dagger c_{n+1}. \quad (\text{A3})$$

The quadratic terms in fermions can be diagonalized by a Bogoliubov transformation (15). The resulting free-fermion dispersion is different from Eq. (16). Expressing the interaction part in terms of Bogoliubov fermions and normal ordering self-consistently leads to a theory of the same structure as the one derived in Sec. III. In fact we expect it to be identical, but we have not verified this.

APPENDIX B: ONE-VERTEX DIAGRAMS

In this section we list the first-order contributions to the transverse response and discuss their divergent behavior.

1. Connected bubble diagrams

The contributions to $L_i^k \Pi_{ij}^{kq}(\omega, Q) R_j^q$ given by connecting two bubbles are (the box vertices in the diagrams indicate the inclusion of the external factors, L_i^k and R_j^q)

$$\text{Diagram 1} = \frac{1}{N^2} \sum_{k,q} \sin(\gamma_k) \sin(\gamma_q) V_2(-k, k+Q, q, -q-Q) \frac{n_k + n_{k+Q} - 1}{i\omega_n - \epsilon_k - \epsilon_{k+Q}} \frac{n_q + n_{q+Q} - 1}{i\omega_n - \epsilon_q - \epsilon_{q+Q}}, \quad (\text{B1})$$

$$\text{Diagram 2} = \frac{1}{N^2} \sum_{k,q} \sin(\gamma_k) \sin(\gamma_q) V_2(q, -q-Q, -k, k+Q) \frac{n_k + n_{k+Q} - 1}{i\omega_n + \epsilon_k + \epsilon_{k+Q}} \frac{n_q + n_{q+Q} - 1}{i\omega_n + \epsilon_q + \epsilon_{q+Q}}, \quad (\text{B2})$$

$$\text{Diagram 1} = \frac{4}{N^2} \sum_{k,q} \cos(\gamma_k) \cos(\gamma_q) V_2(k+Q, q, -k, -q-Q) \frac{n_k - n_{k+Q}}{i\omega_n + \epsilon_k - \epsilon_{k+Q}} \frac{n_q - n_{q+Q}}{i\omega_n + \epsilon_q - \epsilon_{q+Q}}, \quad (\text{B3})$$

$$\text{Diagram 2} = \frac{6}{N^2} \sum_{k,q} \sin(\gamma_k) \sin(\gamma_q) V_0(-k, k+Q, q, -q-Q) \frac{n_k + n_{k+Q} - 1}{i\omega_n + \epsilon_k + \epsilon_{k+Q}} \frac{n_q + n_{q+Q} - 1}{i\omega_n - \epsilon_q - \epsilon_{q+Q}}, \quad (\text{B4})$$

$$\text{Diagram 3} = \frac{6}{N^2} \sum_{k,q} \sin(\gamma_k) \sin(\gamma_q) V_0(-k, k+Q, q, -q-Q) \frac{n_k + n_{k+Q} - 1}{i\omega_n - \epsilon_k - \epsilon_{k+Q}} \frac{n_q + n_{q+Q} - 1}{i\omega_n + \epsilon_q + \epsilon_{q+Q}}, \quad (\text{B5})$$

$$\text{Diagram 4} = \frac{6}{N^2} \sum_{k,q} \sin(\gamma_k) \sin(\gamma_q) V_0(-k, k+Q, q, -q-Q) \frac{n_k + n_{k+Q} - 1}{i\omega_n - \epsilon_k - \epsilon_{k+Q}} \frac{n_q + n_{q+Q} - 1}{i\omega_n + \epsilon_q + \epsilon_{q+Q}}, \quad (\text{B6})$$

$$\text{Diagram 5} = -\frac{3}{N^2} \sum_{k,q} \sin(\gamma_k) \cos(\gamma_q) iV_1(-q, q+Q, -k-Q, k) \frac{n_k + n_{k+Q} - 1}{i\omega_n - \epsilon_k - \epsilon_{k+Q}} \frac{n_q - n_{q+Q}}{i\omega_n - \epsilon_q + \epsilon_{q+Q}}, \quad (\text{B7})$$

$$\text{Diagram 6} = \frac{3}{N^2} \sum_{k,q} \cos(\gamma_k) \sin(\gamma_q) iV_1^*(k+Q, -k, q, -q-Q) \frac{n_k - n_{k+Q}}{i\omega_n + \epsilon_k - \epsilon_{k+Q}} \frac{n_q + n_{q+Q} - 1}{i\omega_n - \epsilon_q - \epsilon_{q+Q}}, \quad (\text{B8})$$

$$\text{Diagram 7} = -\frac{3}{N^2} \sum_{k,q} \sin(\gamma_k) \cos(\gamma_q) iV_1^*(-q-Q, -k, k+Q, q) \frac{n_k + n_{k+Q} - 1}{i\omega_n + \epsilon_k + \epsilon_{k+Q}} \frac{n_q - n_{q+Q}}{i\omega_n - \epsilon_q + \epsilon_{q+Q}}. \quad (\text{B9})$$

2. Tadpole-type diagrams

These contributions consist of bubbles in which one of the propagators features a tadpole type self-energy interaction


$$\left[\text{Diagram 8} + \text{Diagram 9} \right] = \frac{8}{N^2} \sum_{k,q} [\cos(2\gamma_k) - 1] \frac{n_q V_2(-k, q, -q, k)}{i\omega_n - \epsilon_k - \epsilon_{k+Q}} \left[\frac{n_k + n_{k+Q} - 1}{i\omega_n - \epsilon_k - \epsilon_{k+Q}} - \beta n_k (1 - n_k) \right], \quad (\text{B10})$$

$$\left[\text{Diagram 10} + \text{Diagram 11} \right] = -\frac{2}{N^2} \sum_{k,q} [\cos(2\gamma_k) - 1] \frac{n_q V_2(k, q, -q, -k)}{i\omega_n + \epsilon_k + \epsilon_{k+Q}} \left[\frac{n_k + n_{k+Q} - 1}{i\omega_n + \epsilon_k + \epsilon_{k+Q}} + \beta n_k (1 - n_k) \right], \quad (\text{B11})$$


$$\begin{aligned} \left[\text{Diagram 12} + \text{Diagram 13} \right] &= \frac{2}{N^2} \sum_{k,q} [\cos(2\gamma_k) + 1] \frac{n_q V_2(k, q, -q, -k)}{i\omega_n + \epsilon_k - \epsilon_{k+Q}} \left[\frac{n_k - n_{k+Q}}{i\omega_n + \epsilon_k - \epsilon_{k+Q}} + \beta n_k (1 - n_k) \right] - \frac{2}{N^2} \sum_{k,q} [\cos(2\gamma_k) \\ &+ 1] \frac{n_q V_2(k+Q, q, -q, -k-Q)}{i\omega_n + \epsilon_k - \epsilon_{k+Q}} \left[\frac{n_k - n_{k+Q}}{i\omega_n + \epsilon_k - \epsilon_{k+Q}} + \beta n_{k+Q} (1 - n_{k+Q}) \right], \end{aligned} \quad (\text{B12})$$

$$\left[\text{Diagram 14} \right] = -\frac{3}{N^2} \sum_{k,q} \sin(2\gamma_k) iV_1(q, -q, -k, k) \frac{n_q}{i\omega_n + \epsilon_k - \epsilon_{k+Q}} \left[\frac{n_k + n_{k+Q} - 1}{i\omega_n - \epsilon_k - \epsilon_{k+Q}} + \frac{2n(\epsilon_k) - 1}{2\epsilon_k} \right], \quad (\text{B13})$$

$$\left[\text{Diagram 15} \right] = -\frac{3}{N^2} \sum_{k,q} \sin(2\gamma_k) iV_1(q, -q, -k, k) \frac{n_q}{i\omega_n + \epsilon_k + \epsilon_{k+Q}} \left[\frac{n_k - n_{k+Q}}{i\omega_n - \epsilon_k + \epsilon_{k+Q}} + \frac{2n(\epsilon_k) - 1}{2\epsilon_k} \right], \quad (\text{B14})$$



$$\left[\text{Diagram} \right] = \frac{3}{N^2} \sum_{k,q} \sin(2\gamma_k) iV_1(q, -q, -k, k) \frac{n_q}{i\omega_n - \epsilon_k - \epsilon_{k+Q}} \left[\frac{n_k - n_{k+Q}}{i\omega_n + \epsilon_k - \epsilon_{k+Q}} - \frac{2n(\epsilon_k) - 1}{2\epsilon_k} \right], \quad (\text{B15})$$



$$\left[\text{Diagram} \right] = -\frac{3}{N^2} \sum_{k,q} \sin(2\gamma_k) iV_1(q, -q, -k, k) \frac{n_q}{i\omega_n - \epsilon_k + \epsilon_{k+Q}} \left[\frac{n_k + n_{k+Q} - 1}{i\omega_n + \epsilon_k + \epsilon_{k+Q}} - \frac{2n(\epsilon_k) - 1}{2\epsilon_k} \right]. \quad (\text{B16})$$

One expects that, just as at zeroth order, these diagrams will have divergences at certain energies. Inspection of the pole structure of the connected bubble diagrams [Eqs. (B1)–(B9)] suggests that they will have stronger divergences than the zeroth order because they feature products of poles. Numerical results support this assumption for Eqs. (B1) and (B2). On the other hand, it is clear that Eqs. (B4)–(B9) will be very small (for large Δ) because they contain products of terms that, individually, are only significant for different discrete regions in ω . The behavior of Eq. (B3) is subtler. This diagram gives the most significant first-order contribution to the response at $\omega \sim 0$. However it does not contain a stronger divergence than its zeroth-order equivalent. The reason is as follows. Consider the sum

$$\sum_k \frac{I(k, Q)}{\omega + \epsilon_k - \epsilon_{k+Q} + i\eta}, \quad (\text{B17})$$

with $I(k, Q)$ an analytic function of k, Q . As shown at zeroth order, because the dispersion ϵ_k is bounded, the imaginary part of the sum (as $\eta \rightarrow 0$) will in turn be bounded. In general there is a divergence at the threshold $\omega = \max(\epsilon_k - \epsilon_{k+Q})$ of the corresponding response. Naively one then expects that in the double sum

$$\sum_{k,q} \frac{I(k, Q)I(q, Q)I'(k, q, Q)}{(\omega + \epsilon_k - \epsilon_{k+Q} + i\eta)(\omega + \epsilon_q - \epsilon_{q+Q} + i\eta)}, \quad (\text{B18})$$

with $I'(k, q, Q)$ analytic, the maximum contribution will occur for $k=q$ and $\omega = \max(\epsilon_k - \epsilon_{k+Q})$. For Eq. (B3) the function $V_2(k+Q, k, -k, -k-Q)$ vanishes at the threshold $\omega = \max(\epsilon_k - \epsilon_{k+Q})$. This means that the divergence is in fact substantially weaker than at zeroth order. This behavior does not persist when self-energy corrections to the propagator are included. This is because the self-energy corrections shift the thresholds of the response. Stronger than leading-order divergences are also found in Eqs. (B10)–(B16). To take them into account the single-particle propagator must be resummed using a Dyson equation, as in Sec. V D.

APPENDIX C: MATRIX STRUCTURE OF THE BUBBLE SUMMATION

In this appendix we show that summing all bubble diagrams results in the integral Eq. (65) for the matrix Π^{RPA} . The proof follows by induction. Our starting point is expressions (39) and (42) for the dynamical susceptibility. The n th order contribution to the matrix Π is by definition

$$-\langle T_\tau \mathbf{X}(\tau, Q|k) \mathbf{X}^\dagger(0, Q|q) U^{(n)} \rangle, \quad (\text{C1})$$

where

$$U^{(n)} = \frac{(-1)^n}{n!} \prod_{m=1}^n \int_0^\beta d\tau_m H_4'(\tau_m). \quad (\text{C2})$$

Out of all possible contractions in Eq. (C1) we want to select only those that give rise to bubble diagrams. We denote their contribution by $\Pi_{(n)}^{\text{RPA}}$. We wish to show that

$$\Pi_{(n)}^{\text{RPA}}(\tau, Q|k, q) = (\mathbf{K} \circ \mathbf{K} \circ \dots \circ \mathbf{K} \circ \Pi^0)(\tau, Q|k, q), \quad (\text{C3})$$

where \mathbf{K} is defined as

$$K_{\alpha\beta}(\tau, Q|k, q) = \sum_{k'} \Pi_{\alpha\gamma}^0(\tau, Q|k, k') V_{\gamma\beta}(Q|k', q) \quad (\text{C4})$$

and \circ denotes a convolution and simultaneous matrix multiplication

$$\begin{aligned} (\mathbf{K} \circ \mathbf{K})_{\alpha\beta}(\tau, Q|k, q) \\ = \frac{1}{N} \sum_{k'} \int d\tau_1 K_{\alpha\gamma}(\tau - \tau_1, Q|k, k') K_{\gamma\beta}(\tau_1, Q|k', q). \end{aligned} \quad (\text{C5})$$

Fourier transforming (C3) then gives

$$\Pi_{(n)}^{\text{RPA}}(i\omega_n, Q|k, q) = (\mathbf{K} * \mathbf{K} * \dots * \mathbf{K} * \Pi^0)(i\omega_n, Q|k, q), \quad (\text{C6})$$

where the convolution $*$ is defined as

$$\begin{aligned} (\mathbf{K} * \mathbf{K})_{\alpha\beta}(i\omega_n, Q|k, q) \\ = \frac{1}{N} \sum_{k'} K_{\alpha\gamma}(i\omega_n, Q|k, k') K_{\gamma\beta}(i\omega_n, Q|k', q). \end{aligned} \quad (\text{C7})$$

Summing over n then leads to

$$\Pi^{\text{RPA}}(i\omega_n, Q|k, q) = \sum_{n=0}^{\infty} \Pi_{(n)}^{\text{RPA}}(i\omega_n, Q|k, q). \quad (\text{C8})$$

This can be written as

$$\Pi^{\text{RPA}} = \sum_{n=0}^{\infty} \mathbf{K}^n * \Pi^0 = (\mathbf{I} - \mathbf{K})^{-1} * \Pi^0, \quad (\text{C9})$$

where

$$\mathbf{K}^n = \overbrace{\mathbf{K} * \mathbf{K} \cdots * \mathbf{K}}^n. \quad (\text{C10})$$

The basic identity underlying the inductive proof of Eq. (C3) is

$$\overline{\mathbf{X}(\tau, Q|k)U^{(n)}}|_{\text{RPA}} = (\mathbf{K} \circ \mathbf{K} \circ \cdots \circ \mathbf{K} \circ \mathbf{X})(\tau, Q|k), \quad (\text{C11})$$

where the contraction notation indicates that only contractions compatible with our RPA-like summation have been carried out. Equation (C3) is clearly a direct consequence of Eq. (C11). We now prove Eq. (C11) by induction. For $n=1$ we prove by a lengthy but straightforward calculation that

$$\overline{\mathbf{X}(\tau, Q|k)U^{(1)}}|_{\text{RPA}} = (\mathbf{K} \circ \mathbf{X})(\tau, Q|k). \quad (\text{C12})$$

The induction step is then straightforward. We have

$$\overline{\mathbf{X}(\tau, Q|k)U^{(n+1)}}|_{\text{RPA}} = - \int d\tau_{n+1} \overline{\mathbf{Y}H'_4(\tau_{n+1})}|_{\text{RPA}}, \quad (\text{C13})$$

where

$$\mathbf{Y} = \overline{\mathbf{X}(\tau, Q|k)U^{(n)}}|_{\text{RPA}}. \quad (\text{C14})$$

The combinatorial factor $n+1$ cancels exactly against the $1/(n+1)$ in the definition of $U^{(n+1)}$. Now using the induction assumption (C11) in Eq. (C14), the final contraction in Eq. (C13) reduces to the induction start $n=1$, thus establishing the validity of Eq. (C11) for $n+1$.

APPENDIX D: ELEMENTS OF Π_S

Introducing the definitions

$$B_{--}(k, k+Q) = - \frac{n(E_k) + n(E_{k+Q}) - 1}{i\omega_n - E_k - E_{k+Q}}, \quad (\text{D1})$$

$$B_{++}(k, k+Q) = - \frac{1 - n(E_k) - n(E_{k+Q})}{i\omega_n + E_k + E_{k+Q}}, \quad (\text{D2})$$

$$B_{-+}(k, k+Q) = - \frac{n(E_k) - n(E_{k+Q})}{i\omega_n - E_k + E_{k+Q}}, \quad (\text{D3})$$

$$B_{+-}(k, k+Q) = - \frac{n(E_{k+Q}) - n(E_k)}{i\omega_n + E_k - E_{k+Q}}, \quad (\text{D4})$$

the explicit elements of the matrix, Eq. (89), are

$$\begin{aligned} \Pi_{11}^S(i\omega_n, Q|k, k') &= \sum_{\sigma, \sigma'=\pm} Z_k^\sigma Z_{k+Q}^{\sigma'} B_{\sigma\sigma'}(k, k+Q) (\delta_{k, k'} \\ &\quad - \delta_{k, -k'-Q}), \end{aligned} \quad (\text{D5})$$

$$\begin{aligned} \Pi_{12}^S(i\omega_n, Q|k, k') &= \sum_{\sigma, \sigma'=\pm} \sigma \lambda_{k'} Z_{k'+Q}^{\sigma'} B_{\sigma\sigma'}(k', k'+Q) (\delta_{k, k'} \\ &\quad - \delta_{k, -k'-Q}), \end{aligned} \quad (\text{D6})$$

$$\begin{aligned} \Pi_{13}^S(i\omega_n, Q|k, k') &= \sum_{\sigma, \sigma'=\pm} \sigma \sigma' \lambda_{k+Q} \lambda_k B_{\sigma\sigma'}(k, k+Q) (\delta_{k, k'} \\ &\quad - \delta_{k, -k'-Q}), \end{aligned} \quad (\text{D7})$$

$$\begin{aligned} \Pi_{21}^S(i\omega_n, Q|k, k') &= - \sum_{\sigma, \sigma'=\pm} \sigma \lambda_k Z_{k+Q}^{\sigma'} B_{\sigma\sigma'}(k, k+Q) (\delta_{k, k'} \\ &\quad - \delta_{k, -k'-Q}), \end{aligned} \quad (\text{D8})$$

$$\begin{aligned} \Pi_{22}^S(i\omega_n, Q|k, k') &= \sum_{\sigma, \sigma'=\pm} (Z_{k+Q}^{\sigma'} Z_k^\sigma \delta_{k, k'} \\ &\quad + \sigma \sigma' \lambda_k \lambda_{k+Q} \delta_{k, -k'-Q}) B_{\sigma\sigma'}(k, k+Q), \end{aligned} \quad (\text{D9})$$

$$\begin{aligned} \Pi_{23}^S(i\omega_n, Q|k, k') &= \sum_{\sigma, \sigma'=\pm} \sigma' \lambda_{k+Q} Z_k^\sigma B_{\sigma\sigma'}(k, k+Q) (\delta_{k, k'} \\ &\quad - \delta_{k, -k'-Q}), \end{aligned} \quad (\text{D10})$$

$$\begin{aligned} \Pi_{31}^S(i\omega_n, Q|k, k') &= \sum_{\sigma, \sigma'=\pm} \sigma \sigma' \lambda_{k+Q} \lambda_k B_{\sigma\sigma'}(k, k+Q) (\delta_{k, k'} \\ &\quad - \delta_{k, -k'-Q}), \end{aligned} \quad (\text{D11})$$

$$\begin{aligned} \Pi_{32}^S(i\omega_n, Q|k, k') &= - \sum_{\sigma, \sigma'=\pm} \sigma' \lambda_{k'+Q} Z_{k'}^\sigma B_{\sigma\sigma'}(k', k'+Q) (\delta_{k, k'} \\ &\quad - \delta_{k, -k'-Q}), \end{aligned} \quad (\text{D12})$$

$$\begin{aligned} \Pi_{33}^S(i\omega_n, Q|k, k') &= \sum_{\sigma, \sigma'=\pm} Z_k^\sigma Z_{k+Q}^{\sigma'} B_{\sigma\sigma'}(k, k+Q) (\delta_{k, k'} \\ &\quad - \delta_{k, -k'-Q}). \end{aligned} \quad (\text{D13})$$

APPENDIX E: FURTHER CONTRIBUTIONS TO THE XXZ SPIN CHAIN RESPONSE

The calculation described in the main text leads to a response that features sharp thresholds even at finite temperature. Physically one expects these thresholds to be absent at $T \neq 0$. The diagrams we consider are incapable of capturing this effect because they include poles that only depend on two single-particle energies. This limits the response at positive frequencies to the regions $\min(E_k + E_q) \leq \omega \leq \max(E_k + E_q)$ and $0 \leq \omega \leq \max(E_k - E_q)$ for general k, q . Coupling to decay channels involving more than two particles should alleviate this problem.

One can evaluate the two-loop self-energy correction to the propagator. This includes diagrams of the form



$$, \dots \quad (\text{E1})$$

In analogy with the one-loop calculation, we define a self-energy matrix Σ_2 . As before the transferred frequency and

momentum are labeled by ik_n and k , respectively. Defining $r=k+p+q$, the elements of the matrix Σ_2^{ij} are

$$\begin{aligned} \Sigma_2^{12} = & -\frac{24}{N^2} \sum_{p,q} \tilde{V}_1(k, -r, p, q) \tilde{V}_0(k, \\ & -r, p, q) \frac{n(\epsilon_q) + n(\epsilon_r) - 1}{ik_n + \epsilon_p + \epsilon_q + \epsilon_r} [n(\epsilon_p) - n_B(\epsilon_q + \epsilon_r) - 1] \\ & -\frac{24}{N^2} \sum_{p,q} \tilde{V}_1(k, -r, p, q) \tilde{V}_0(-q, -p, r, \\ & -k) \frac{n(\epsilon_q) + n(\epsilon_r) - 1}{ik_n - \epsilon_p - \epsilon_q - \epsilon_r} [n(\epsilon_p) - n_B(\epsilon_q + \epsilon_r) - 1] \\ & +\frac{12}{N^2} \sum_{p,q} \tilde{V}_1^*(r, -p, -q, -k) \tilde{V}_2(r, -k, -p, \\ & -q) \frac{n(\epsilon_q) - n(\epsilon_r)}{ik_n + \epsilon_p + \epsilon_q - \epsilon_r} [n(\epsilon_p) + n_B(\epsilon_r - \epsilon_q)] \\ & +\frac{12}{N^2} \sum_{p,q} \tilde{V}_1^*(r, -p, -q, -k) \tilde{V}_2(k, \\ & -r, p, q) \frac{n(\epsilon_q) - n(\epsilon_r)}{ik_n - \epsilon_p - \epsilon_q + \epsilon_r} [n(\epsilon_p) + n_B(\epsilon_r - \epsilon_q)], \quad (E2) \end{aligned}$$

$$\begin{aligned} \Sigma_2^{11} = & \frac{96}{N^2} \sum_{p,q} [\tilde{V}_0(k, -r, p, q)]^2 \frac{n(\epsilon_q) + n(\epsilon_r) - 1}{ik_n + \epsilon_p + \epsilon_q + \epsilon_r} [n(\epsilon_p) - n_B(\epsilon_q \\ & + \epsilon_r) - 1] + \frac{6}{N^2} \sum_{p,q} |\tilde{V}_1(k, \\ & -r, p, q)|^2 \frac{n(\epsilon_q) + n(\epsilon_r) - 1}{ik_n - \epsilon_p - \epsilon_q - \epsilon_r} [n(\epsilon_p) - n_B(\epsilon_q + \epsilon_r) - 1] \end{aligned}$$

$$\begin{aligned} & +\frac{18}{N^2} \sum_{p,q} |\tilde{V}_1(r, -q, -p, -k)|^2 \frac{n(\epsilon_q) - n(\epsilon_r)}{ik_n + \epsilon_p + \epsilon_q - \epsilon_r} [n(\epsilon_p) \\ & + n_B(\epsilon_r - \epsilon_q)] + \frac{8}{N^2} \sum_{p,q} [\tilde{V}_2(k, \\ & -r, p, q)]^2 \frac{n(\epsilon_q) - n(\epsilon_r)}{ik_n - \epsilon_p - \epsilon_q + \epsilon_r} [n(\epsilon_p) + n_B(\epsilon_r - \epsilon_q)]. \quad (E3) \end{aligned}$$

Here we have used the boson occupation factor, $n_B(\epsilon) = 1/[\exp(\beta\epsilon) - 1]$. The remaining elements of the two-loop self-energy are obtained via

$$\Sigma_2^{22} = -(\Sigma_2^{11})^*, \quad (E4)$$

$$\Sigma_2^{21} = (\Sigma_2^{12})^*. \quad (E5)$$

These contributions have poles that feature three single-particle energies. Some of these contributions will lead to a temperature-dependent broadening of the response in the vicinities of $\omega \sim \Delta J$ and $\omega \sim 0$. Including the two-loop self-energy terms should further increase the quality of our approximation. However the extra sum over the loop momentum means that such a computation would be a factor of $N \sim 400$ slower.

-
- ¹R. Orbach, Phys. Rev. **112**, 309 (1958).
²J. Des Cloizeaux and M. Gaudin, J. Math. Phys. **7**, 1384 (1966).
³C. N. Yang and C. P. Yang, Phys. Rev. **150**, 321 (1966).
⁴V. E. Korepin, N. M. Bogoliubov, and A. G. Izergin, *Quantum Inverse Scattering Method and Correlation Functions* (Cambridge University Press, Cambridge, England, 1993).
⁵H. A. Algra, L. J. de Jongh, H. W. J. Blöte, W. J. Huiskamp, and R. L. Carlin, Physica B & C **82**, 239 (1976).
⁶P. M. Duxbury, J. Oitmaa, M. N. Barber, A. van der Bilt, K. O. Joungh, and R. L. Carlin, Phys. Rev. B **24**, 5149 (1981).
⁷H. Yoshizawa, G. Shirane, H. Shiba, and K. Hirakawa, Phys. Rev. B **28**, 3904 (1983).
⁸S. E. Nagler, W. J. L. Buyers, R. L. Armstrong, and B. Briat, Phys. Rev. Lett. **49**, 590 (1982).
⁹S. E. Nagler, W. J. L. Buyers, R. L. Armstrong, and B. Briat, Phys. Rev. B **28**, 3873 (1983).
¹⁰H. Yoshizawa, K. Hirakawa, S. K. Satija, and G. Shirane, Phys. Rev. B **23**, 2298 (1981).
¹¹A. Oosawa, K. Kakurai, Y. Nishiwaki, and T. Kato, J. Phys. Soc. Jpn. **75**, 074719 (2006).
¹²L. D. Faddeev and L. A. Takhtajan, Phys. Lett. **85A**, 375 (1981).
¹³H.-B. Braun, J. Kulda, B. Roessli, D. Visser, K. W. Krämer, H.-U. Güdel, and P. Böni, Nat. Phys. **1**, 159 (2005).
¹⁴I. Zalitznyak and S. Lee, in *Magnetic Neutron Scattering in Modern Techniques for Characterizing Magnetic Materials*, edited by Y. Zhu (Springer, New York, 2005).
¹⁵J. Villain, Physica B & C **79**, 1 (1975).
¹⁶F. H. L. Essler and R. M. Konik, Phys. Rev. B **78**, 100403(R) (2008).
¹⁷A. J. A. James, F. H. L. Essler, and R. M. Konik, Phys. Rev. B **78**, 094411 (2008).
¹⁸H. J. Mikeska and C. Luckmann, Phys. Rev. B **73**, 184426 (2006).
¹⁹D. A. Tennant *et al.* (unpublished).
²⁰E. Lieb, T. Schultz, and D. Mattis, Ann. Phys. (N.Y.) **16**, 407 (1961).
²¹Th. Niemeijer, Physica (Amsterdam) **36**, 377 (1967); **39**, 313 (1968).
²²H. G. Vaidya and C. A. Tracy, Physica A **92**, 1 (1978).
²³B. M. McCoy, Phys. Rev. **173**, 531 (1968); E. Barouch and B. M. McCoy, Phys. Rev. A **3**, 786 (1971); B. M. McCoy, E. Barouch, and D. B. Abraham, *ibid.* **4**, 2331 (1971); G. Müller

- and R. E. Shrock, Phys. Rev. Lett. **51**, 219 (1983); J. Appl. Phys. **55**, 1874 (1984).
- ²⁴N. Ishimura and H. Shiba, Prog. Theor. Phys. **63**, 743 (1980).
- ²⁵H. J. Mikeska, Phys. Rev. B **12**, 2794 (1975).
- ²⁶J.-S. Caux, J. Mossel, and I. Pérez Castillo, J. Stat. Mech.: Theory Exp. **2008**, P08006.
- ²⁷M. Jimbo and T. Miwa, *Algebraic Analysis of Solvable Lattice Models* (American Mathematical Society, Providence, 1995).
- ²⁸A. H. Bougourzi, M. Karbach, and G. Müller, Phys. Rev. B **57**, 11429 (1998).
- ²⁹M. Takahashi, Prog. Theor. Phys. **46**, 401 (1971); M. Takahashi and M. Suzuki, *ibid.* **48**, 2187 (1972); C. Destri and H. J. de Vega, Phys. Rev. Lett. **69**, 2313 (1992); A. Klümper, Z. Phys. B: Condens. Matter **91**, 507 (1993); C. Destri and H. J. de Vega, Nucl. Phys. B **438**, 413 (1995); K. Fabricius, A. Klümper, and B. M. McCoy, Phys. Rev. Lett. **82**, 5365 (1999).
- ³⁰F. H. L. Essler, H. Frahm, F. Göhmann, A. Klümper, and V. E. Korepin, *The One-Dimensional Hubbard Model* (Cambridge University Press, Cambridge, England, 2005).
- ³¹M. Takahashi, *Thermodynamics of One-Dimensional Solvable Models* (Cambridge University Press, Cambridge, England, 2005).
- ³²J. D. Johnson, J. Appl. Phys. **52**, 1991 (1981).
- ³³N. Kitanine, J. M. Maillet, N. A. Slavnov, and V. Terras, Nucl. Phys. B **729**, 558 (2005).
- ³⁴F. Göhmann, A. Klümper, and A. Seel, J. Phys. A **37**, 7625 (2004).
- ³⁵F. Göhmann, N. P. Hasenclever, and A. Seel, J. Stat. Mech.: Theory Exp. **2005**, P10015.
- ³⁶K. Sakai, J. Phys. A: Math. Theor. **40**, 7523 (2007).
- ³⁷K. Fabricius, U. Löw, and J. Stolze, Phys. Rev. B **55**, 5833 (1997); S. Grossjohann and W. Brenig, *ibid.* **79**, 094409 (2009); T. Barthel, U. Schollwöck, and S. White, arXiv:0901.2342 (unpublished).
- ³⁸P. Jordan and E. Wigner, Z. Phys. **47**, 631 (1928).
- ³⁹H. A. Kramers and G. H. Wannier, Phys. Rev. **60**, 252 (1941).
- ⁴⁰G. Gómez-Santos, Phys. Rev. B **41**, 6788 (1990).
- ⁴¹D. V. Dmitriev, V. Y. Krivnov, and A. A. Ovchinnikov, Phys. Rev. B **65**, 172409 (2002); D. V. Dmitriev, V. Ya. Krivnov, A. A. Ovchinnikov, and A. Langari, JETP **95**, 538 (2002); J.-S. Caux, F. H. L. Essler, and U. Löw, Phys. Rev. B **68**, 134431 (2003); F. Capraro and C. Gros, Eur. Phys. J. B **29**, 35 (2002); R. Hagemans, J. S. Caux, and U. Löw, Phys. Rev. B **71**, 014437 (2005).
- ⁴²J. B. Kogut, Rev. Mod. Phys. **51**, 659 (1979).
- ⁴³G. Müller, H. Thomas, H. Beck, and J. C. Bonner, Phys. Rev. B **24**, 1429 (1981).